Chapter 1

A general overview of high-energy heavy-ion interaction

1.1 Introduction

The standard model (SM) of particle physics is basically a reductionist approach, that explains the dynamics of quarks and leptons, the most fundamental building blocks of all material objects that we see in nature [1–3]. In particular the dynamics of quarks and gluons, the constituent particles (fields) of hadrons, are guided by Quantum Chromodynamics (QCD), a non-abelian quantum field theory based on the $SU_c(3)$ color gauge group that describes the physics of strong interaction [4]. Unlike the photons in quantum electrodynamics (QED), the gluons are self interacting, which gives rise to two very special features of strong interaction, namely the asymptotic freedom [5, 6] and color confinement [7]. Because the gluons themselves have color, it leads to an anti-screening of the color charge. The bare color charge of a quark seated at the origin is diluted away in space by the gluons. If one tries to see the bare charge of the quark through the surrounding gluonic field, one will actually be able to see only a small portion of it. This feature of color fields is reflected in the behavior of the dimensionless coupling constant α_s, that determines the dynamics of strong interaction. Using the renormalization technique, formal infinities in α_s arising out of momentum contributions coming from virtual particles, are traded for a finite value,

$$\alpha_s(Q^2) = \frac{12\pi}{\beta_0 \ln\left(\frac{Q^2}{\Lambda^2_{qcd}}\right)} \tag{1.1}$$

upto the second order in perturbation theory. Here Q is the 4-momentum transfer, Λ_{qcd} $= (0.1 - 0.5)$ GeV, is a characteristic cut off scale of strong interaction down to which the perturbation theory works, $\beta_0 = 33 - 2N_f$ is the first coefficient of the β-function – higher order coefficients are neglected due to renormalization, and N_f is the effective number of quark flavors present in the system. In Figure 1.1 values of α_s, extracted from different experiments, are plotted against Q, and as we can see the experimental values are quite nicely reproduced by the Lattice QCD calculation [8]. In the $Q^2 \gg \Lambda^2_{qcd}$ region the strength

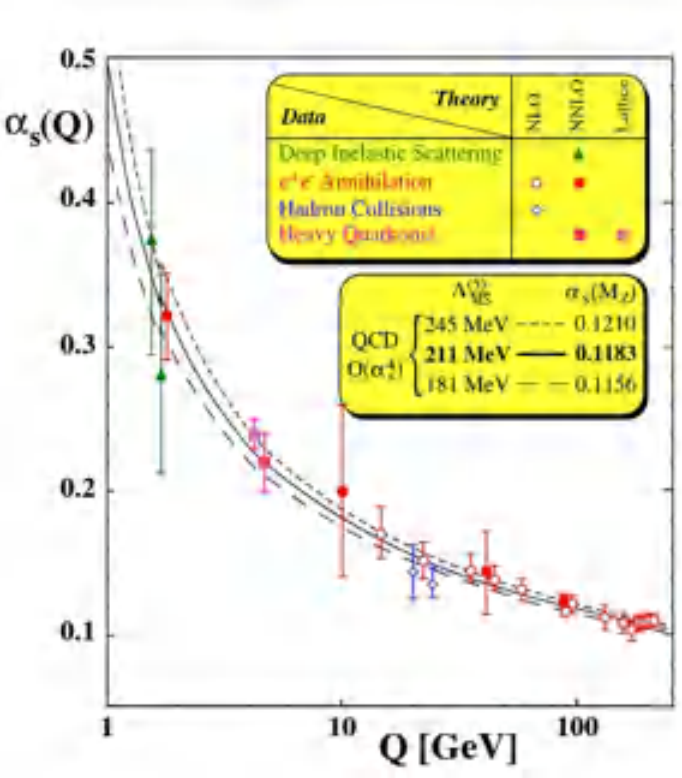

Figure 1.1: Measurements of the strong field coupling constant (α_s) against energy-momentum transfer Q. Lines refer to the perturbative QCD prediction which are in excellent agreement with the experiments. The figure is taken from [8].

of α_s decreases logarithmatically with Q^2. At large momentum transfer or equivalently at short distances the coupling between quarks (and gluons) becomes small, and they are asymptotically free. The phenomenon is known as *asymptotic freedom*. Asymptotic freedom provides a very simple description of how quarks and gluons interact over distance scales $\lesssim 1$ fm, i.e. as long as they are inside a nucleon. However, as Q^2 decreases down to Λ^2_{qcd}, the value of α_s becomes of the order of 1, and the perturbative calculation that leads to Equation (1.1), falls through. We can try to gain some physical insight in the $Q^2 \to 0$ limit by using a simple model proposed in [9, 10]. According to this model, the color potential between a quark (q) and an antiquark ($\bar{q}$) at rest with respect to each other can be written

as,

$$V(r) = -\frac{4\alpha_s}{3r} + \kappa\, r \tag{1.2}$$

where $\alpha_s = g^2/4\pi$ and g is the strength of color charge. The first term of Equation (1.2) represents a normal Coulomb-like force which gives rise to the dipolar lines of force as in the QED. At large r the second term takes over, implying that the $q\bar{q}$-potential rises linearly with separation, and that the field strength remains constant. A flux tube fills up the intervening space of the $q\bar{q}$-system, and the energy required to completely separate the $q\bar{q}$-pair becomes infinite. However, when the energy stored in the flux tube exceeds twice the rest energy of a quark, a new $q\bar{q}$-pair is produced, with the new particles acting either as the source or the sink for the flux lines. Hadrons remain as color neutral objects and free quarks and gluons have never been observed in experiments. Although the model provides a nice intuitive picture, it is hard to quantify. Rigorously explaining the *color confinement* of massive quarks remains hitherto an unresolved problem. High energy hadronic/nuclear collisions can be studied in the framework of QCD using quarks and gluons as the primary degrees of freedom. The final observables in the laboratory are however jets of composite hadrons originating presumably from the struck quarks and radiating gluons. Hadronization, or the process by which the leading high momentum quark leaves behind a trail of $q\bar{q}$-pairs, is modeled by fragmentation functions which are understood only up to a phenomenological level [11].

It was recognized that the QCD implies existence of a new high temperature phase of weakly interacting quarks and gluons [12–14]. However, the idea of a limiting temperature (T_c) for color neutral hadronic matter predates the discovery of QCD, and a quantitative prediction $T_c = 170$ MeV was obtained in the statistical bootstrap model proposed by R. Hagedron [15]. The measured density of hadronic states grows exponentially as,

$$\frac{d\rho}{dm} \sim m^{\alpha}\, \exp\left(\frac{m}{m_0}\right) \tag{1.3}$$

where m represents the mass of the observed hadron and α is a parameter. Using the methods based on statistical mechanics Hagedorn showed that this exponential behavior implies a limiting temperature beyond which the states cannot be composed of color neutral hadrons. He interpreted this limiting temperature as the melting point of hadrons. Indeed, the observed number of hadronic states within an energy interval E and $E + dE$ can be written as [16],

$$dn(E) \sim dE \int_0^E p\, E\, \frac{d\rho}{dm}\, \exp\left(-\frac{E}{kT}\right) dm \tag{1.4}$$

We can use Equation (1.4) and relativistic energy-momentum relation $E^2 = p^2 + m^2$ to write,

$$dn(E) \sim dE \int_0^E m^\alpha \exp\left(\frac{m}{m_0}\right) \exp\left(-\frac{E}{kT}\right) E\sqrt{E^2 - m^2}\, dm \tag{1.5}$$

In the high-energy limit ($E/m_0 \gg 1$) we may approximate Equation (1.5) and compute the above integral,

$$dn(E) \sim E^{\alpha+3} \sqrt{\frac{\pi\, m_0^3}{2E^3}} \exp\left(\frac{E}{m_0} - \frac{E}{kT}\right) dE \tag{1.6}$$

We observe that the total energy $\int E\, dn(E)$ diverges for $kT > kT_0 = m$. One may therefore conclude that either no temperature beyond T_0 is possible, or there should be some new physics that would describe the states.

If the above does not provide enough motivation to study high-energy collisions of elementary particles and/or nuclei and explore the issues related to color deconfinement, then there are implications of confinement – deconfinement transition in cosmology and astrophysics too. It is believed that at the time of *Big Bang* all four fundamental forces of nature, namely Gravitational, Weak, Electromagnetic and Strong, had equal strengths and were unified into one fundamental interaction [17, 18]. At about 10^{-43} s. after the Big Bang, the gravitational interaction was separated out while the other three remained unified. At about 10^{-36} s. the strong interaction got decoupled from the electromagnetic and weak. Thereafter the universe expanded exponentially, a primordial cosmological phenomenon popularly known as the *cosmic inflation*. This was followed by a radiation dominated thermal era of the universe. As the universe further expanded and lost its temperature, it went through a series of symmetry breaking processes and corresponding phase transitions. Material objects started to evolve in the form of most fundamental particles, namely quarks, antiquarks, and leptons. It is during this stage when the universe was only a few micro-seconds old, the Quark-Gluon Plasma (QGP), a color deconfined, weakly coupled state of quarks and gluons was created [19]. It was a hot QGP where the number densities of quarks and antiquarks were same. For a very brief period of time the quarks and gluons could roam around freely outside the boundaries of hadrons, and the entire universe was filled up with a QGP-like state along with the leptons. However, subsequent expansion and cooling down brought the universe to such a stage that allowed the quarks to coalesce into color neutral baryonic matter like the protons and neutrons. A probable scenario of the expanding universe after the Big Bang and subsequent stages of its evolution are presented in Figure 1.2. A QGP state, similar but not quite alike to that prevailed in the early universe, can also be found inside the cores of very compact astrophysical objects like the white dwarfs and neutron stars [20]. In this case due to enormous (inward) gravitational pressure the boundaries of individual baryons melt down leading to a deconfinement. The temperature however, is

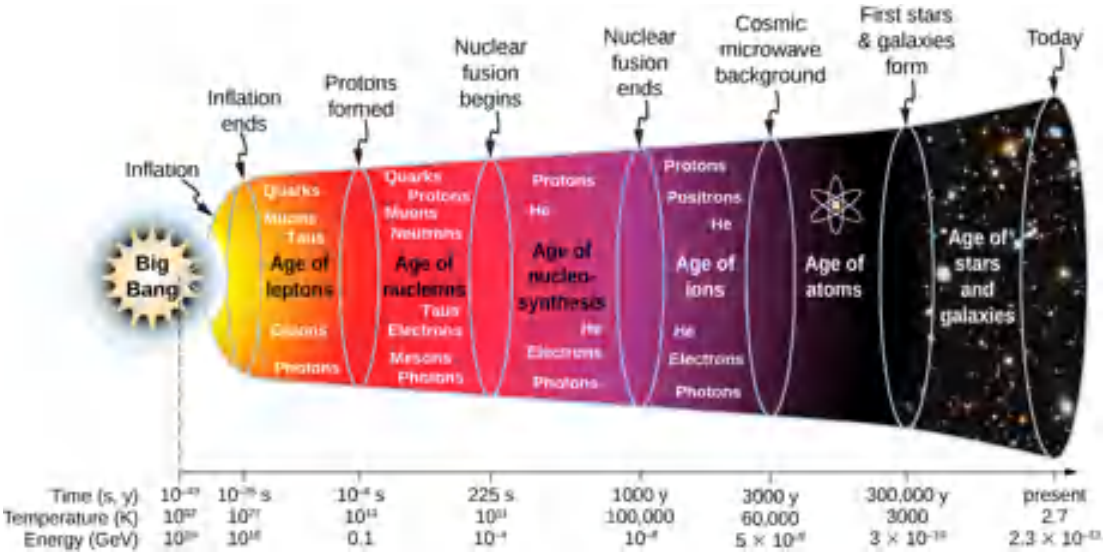

Figure 1.2: A probable timeline of the universe since Big Bang [21].

much below than that of the early universe, the density is $5-10$ times the normal nuclear density, and the QGP system is quite rich in baryons.

It was T. D. Lee who first suggested that by distributing high energy or high nucleon-density over a relatively large volume, it might be possible to restore the broken symmetries and create an ultra-dense state of quark-gluon matter, pertaining to the early universe, a few microseconds after the Big Bang [22]. Later Collins and Pery suggested that existence of abnormally dense matter with deconfined quarks and gluons is an implicit manifestation of the asymptotic freedom [12]. We explore how under the controlled conditions of a laboratory, in high-energy nucleus-nucleus (AB) collisions these two seemingly different approaches can both lead to a deconfined state of quarks and gluons. The nucleons (radius $\sim$ 1 fm) are composite objects, bound states of quarks and gluons. If two heavy-nuclei are allowed to collide with each other at a moderately high-energy, say at $E_{\rm lab} = 30A - 40A$ GeV, they are going to squeeze each other very hard. With increasing pressure/density, the nucleons belonging to each colliding nuclei would thus overlap, until a state is reached in which each quark finds within its immediate vicinity a considerable number of other quarks. There is no way that it can identify which of these had been its partners in a specific nucleon at some other previous state of lower pressure/density. Beyond a certain point, the concept of a hadron thus loses its meaning, and a system of unbound quarks and gluons, quite rich in its net baryon content, is created. However, the energy density and therefore, the temperature of such a deconfined state is not going to be very high. This is called cold compression, a process that might be happening all the time inside compact stars [20].

On the other hand, as a QCD vacuum of finite volume is heated up, only mesonic degrees

of freedom are excited at low temperatures. Abundance of higher baryonic masses is reduced through the Boltzmann factor, the baryonic thermodynamic weight. The interaction between mesons is resonance dominated. All light quark mesonic states, independent of their mass, have the same characteristic size with a radius of about 1 fm. Mesons appear to allow arbitrary overlap, and by increasing the temperature one may be able to create a quite densely populated state of mesons. Once again we have a situation where the hadronic boundaries are going to melt down and a deconfined QCD state with a little or zero net baryon content is created. Such a hot plasma might have filled up our entire universe just a few micro-seconds after its birth, and perhaps have already been created on the earth in high-energy heavy-ion experiments. Nucleons, on the other hand, in addition to a short range repulsion, experience a long range attraction. Both these forces are non-resonant in nature, so that the interaction in baryonic matter at low temperature and high density is quite different from that of the mesons. A nucleon, also with a hadronic radius of about 1 fm, has an effective hard core of about half of its size. Nevertheless with increasing density, be it through heating or compression, a cluster formation eventually leads to more quarks per hadronic volume than meaningful for a partitioning into color-neutral hadrons. In other words, increasing either the temperature T or the baryochemical potential μ_B, both will eventually result in color deconfinement.

1.1.1 Experimental facilities

Before we delve further into the issues related to AB collision and QGP-state, let us have a look at the accelerator facilities that are either being built up at present or were built up in the past. The first ever heavy-ion collisions in laboratory began at the Lawrence Berkeley National Laboratory (LBNL), Berkeley, USA, and at the Joint Institute for Nuclear Research (JINR), Dubna, USSR. Heavy (light) nuclei were accelerated by employing respectively, the Bevatron and Synchrophasotron in a few (several) GeV per nucleon energy range. The experimental data obtained from these experiments were able to address some significant issues related to the collective behavior of nuclear matter and hadron production in AB collisions. The success of LBNL and JINR experiments encouraged the heavy-ion physics community to extend their investigations to higher energies. Accelerator facilities were built up for fixed target experiments at the Alternating Gradient Synchrotron (AGS) at Brookhaven National Laboratory (BNL), USA, and at Super Proton Synchrotron (SPS) at the European Centre of Research in Nuclear Physics (CERN), Switzerland. These facilities were designed to accelerate both light (^{28}Si, ^{16}O, ^{32}S) and heavy (^{197}Au, ^{208}Pb) ions, respectively at ~ 10 GeV/nucleon and $\sim 10^2$ GeV/nucleon incident energies. Some other heavy-ion programmes were also undertaken like one in the Schwer Ionen Synchrotron (SIS-18, and SIS-100) at GSI, Darmstadt, Germany. These fixed target experiments certainly improved our understanding

Table 1.1: Chronological commissioning of HIC accelerator facilities (past and present).

Year	**Accelerator**	**Projectile**	**Maximum Energy**
1975	Synchrophasotron	C, Mg, Ne, Si	4.5A GeV
1984	Bevatron	C, Ca, Kr, U	1 - 2A GeV
1986	AGS	Si	14.6A GeV
1986	SPS	O, S	200A GeV
1990	SIS-18	Ni, Au	2A GeV
1992	AGS	Au	11A GeV
1994	SPS	Pb	200A GeV
2000	RHIC	Au, Cu	$\sqrt{s_{NN}} = 200$ GeV
2008	LHC	Pb, Xe	$\sqrt{s_{NN}} = 5.5$ TeV
2011	SPS (NA61)	Pb, Be, Ar, Xe	158A GeV
2022	NICA	Au	$\sqrt{s_{NN}} = 11$ GeV
2025	SIS-100 (FAIR)	Au, Ca	11A GeV

of the multiparticle dynamics, but hardly provided any clear signal about QGP formation. However, these experiments have definitely provided a direction or clue, regarding exactly where among the debris of several hundreds (thousands) of particles that are produced per event in the final state, one has to look for to find out if a QGP-like state is formed or not. The AGS-SPS experiments also indicated that there is a specific need to scale up the collision energy further by at least a few orders of magnitude. This is possible only by using a collider system, where particle beams coming from two opposite directions collide with each other. The first *AB* collider experiments started collecting data at the Relativistic Heavy Ion Collider (RHIC) built in the year 2000 at BNL, USA, which provided first unambiguous signal of QGP formation. RHIC covered an energy domain of $\sqrt{s_{NN}} = 7.7$ to 200 GeV, and comprised of four experiments (detector systems), namely STAR, PHENIX, PHOBOS, and BRAHMS. In 2009 the largest ever particle accelerator, the Large Hadron Collider (LHC) at CERN came into operation, which was designed to study *AB* collisions upto $\sqrt{s_{NN}} = 5.5$ TeV and *pp* collisions upto $\sqrt{s_{NN}} = 13$ TeV. Like the RHIC, LHC also comprises of four different experiments, namely ALICE, ATLAS, CMS, and LHCb. The data that came out from the LHC experiments are still being analyzed. So far, the results have supplemented the RHIC observation. It has been possible to create a color deconfined extended QCD state of strongly interacting quarks and gluons. The QGP behaves almost (not exactly) like an ideal fluid, that has a very small specific viscosity. In the last decade or so, several projects have been undertaken to examine and explore the other possibility, i.e. QGP at high baryon density and low/moderate temperature. NA61/SHINE is one such facility that at present is operating at the CERN-SPS. Other such facilities are, (i) the Facility for Anti-proton and Ion Research (FAIR) that is being installed near GSI, Darmstadt, and (ii) NICA at JINR, Dubna which is already in operation. Specific information about the projectile ions and collision energies available in these facilities are listed in Table 1.1.

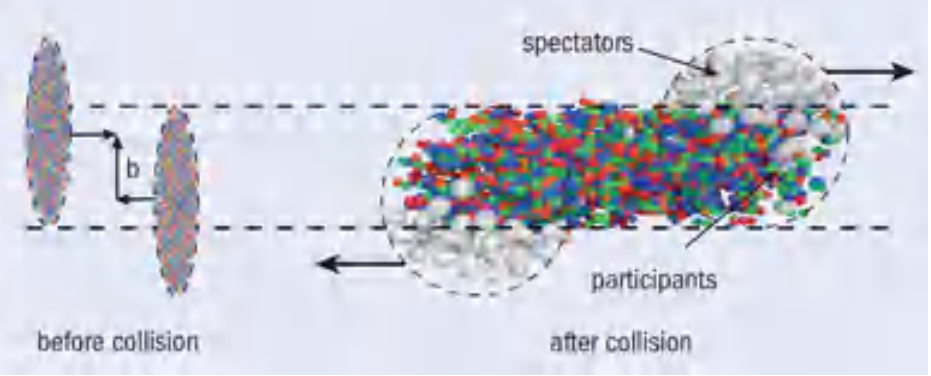

Figure 1.3: A typical nucleus-nucleus interaction before and after the collision. Particles are produced in the participants' zone, while the spectators remain uninfluenced. The figure is taken from Ref. [23].

1.2 Relativistic heavy ion collision and QGP

In its ground state a nucleus of mass number A can be considered like a sphere of radius $R = r_0 A^{1/3}$ fm and volume $V = (4\pi/3) r_0^3 A$, where $r_0 = 1.2$ fm is called the nuclear radius parameter. The nuclear matter density $\rho_{_N} \approx 0.16$ nucleons/fm^3 and the corresponding energy density $\epsilon_{_N} \approx 0.15$ GeV/fm^3. In order to produced a well equilibrated hot and dense fireball matter, for more than one reasons AB collisions are always preferred over pp collisions. First, to achieve a local thermal equilibrium the system must be sufficiently randomized, which is possible only in a large collision system where multiple rescattering among the constituent particles can take place. Second, on an average an AB collision produces a larger number of particles, resulting thereby a smaller amount of relative fluctuation. It is also pertinent to examine how heavy the nucleus should be. The total cross section for $pp \to n\pi$ is ~ 30 mb at high energies, which gives an equilibration time of 6×10^{-34} s. The total time available for hadron production is of the same order as the time for which the colliding nuclei overlap, i.e. $t = 0.2\, r_0\, A^{1/3}/c_s$. Here, $c_s = \sqrt{1/3}\, c$ is the speed of sound in an ideal gas of mesons and nucleons at or near T_c, and the factor 0.2 is incorporated since half the mass of a uniformly dense nucleus is contained within $0.2R$ of its surface. This implies that the disassembly time will be long enough if $A > 50$. Figure 1.3 schematically depicts a high-energy AB event, before and after the collision. Before collision, two such nuclei approaching each other with relativistic speed will look like pancakes, Lorentz contracted along their common (but opposite) direction of motion. The impact parameter (b) of an AB collision is defined as the perpendicular distance between their lines of motion. Head on collisions, also called central events, are associated with small values of b ($b \to 0$), while grazing collisions have high b-values and they are called peripheral events. After the collision takes place, the overlap volume between the two colliding nuclei forms the intermediate fireball. The fireball created in a central and a peripheral collision would be very much different

in their properties, and hence it is essential to study the centrality dependence of different observables. The nucleons inside the overlap region are called *participant* nucleons, whereas those which do not directly participate in the collision process, are called the *spectators*. Often the centrality of a collision is measured in terms of the average number of participant nucleons ($N_{\rm part}$), which varies directly with the mass number of the nuclei. Centrality is also measured in terms of the number of nucleon-nucleon binary collisions ($N_{\rm coll}$) which varies as $A^{4/3}$ [24].

In statistical mechanics the state of a system in local thermal equilibrium, composed of many particles, is characterized by the average values of a few global observables like temperature, energy density, entropy, net charge etc. For different values of these observables, the system may exhibit fundamentally different average properties. Accordingly, there exist different states of matter, and as the system changes from one state to the other, phase transitions take place. Whatever may be the constituent particles, if the intermediate fireball created in an AB collision has to qualify as a state, it should have well defined values of temperature, volume, pressure etc. This is possible only when the motion of the constituent particles is sufficiently random. An order of magnitude calculation in this regard may not be totally out of context. A hadron typically has a radius of 1 fm and it fills up a volume of $5-6$ fm^3. So the hadronic matter density is about $n \sim 0.2$ per fm^3. Typical cross-section of a high-energy hadronic interaction is $\sigma \sim 50$ mbarn or ~ 5 fm^2. Collisions between two heavy-nuclei increase the density by a few orders of magnitude. As a result the hadronic density increases to $n \sim 10$. The mean free path of the constituent particles will therefore be $\lambda \sim (n\sigma)^{-1} \approx 0.02$ fm, and one can expect that multiple ($\sim 10^3$) rescattering are going to take place within a collision volume of dimension $(10-15)$ fm. This with all probability will lead to sufficient randomization of motion of the particles involved, and therefore to an equilibration of the system. The thermodynamic conditions of the intermediate fireball that can be and have been reached in high-energy heavy-ion experiments conducted at the LHC, are listed below [25].

1. Temperature: $T = (100-1000)$ MeV (1 MeV $\equiv$ 10 billion degrees) [up to a million times the temperature of the core of the sun].

2. Pressure: $P = (100-300)$ MeV/fm^3 (1 MeV/fm$^3 \equiv$ 1028 atm.) [pressure at the center of the earth = 3.6 million atm.].

3. Density: $\rho = (5-10)\rho_0$ [ρ_0 is the density of a gold nucleus ~ 3000 g/cm^3; density of a gold atom = 19 g/cm^3].

4. Volume: nearly 1500 fm^3, nucleus radius $R = 1.15 \times A^{1/3}$ fm [for an Au-nucleus $A \approx 200$, $R \simeq 7$ fm and $V = 4\pi R^3/3 \simeq 1500$ fm^3].

5. Duration: $(10 - 50)$ fm/c $\sim 10^{-22}$ s.

6. Baryochemical potential: $\mu_B = (400 - 600)$ GeV.

7. Magnetic field: $B \sim 10^{15} - 10^{16}$ Tesla [in neutron stars $B \sim 10^{11}$ Tesla].

1.2.1 Space-time evolution

As we do not have any direct access to the intermediate fireball, so it is extremely important to understand the space-time evolution of a heavy-ion collision. Figure 1.4 shows different stages of an AB collision system as it evolves with the proper time. The schematic is quite similar to that of the evolving universe after the Big Bang. A schematic representation of

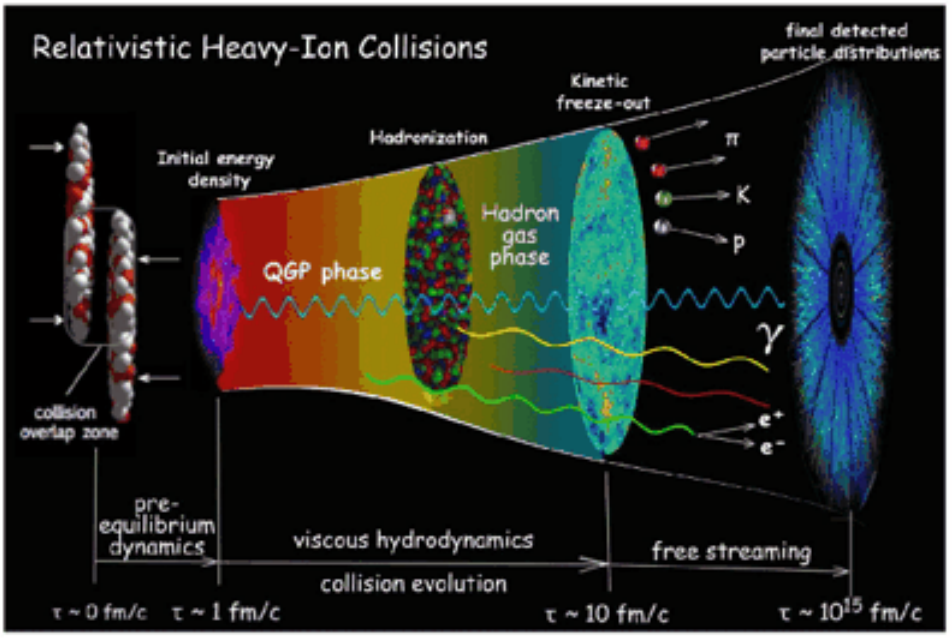

Figure 1.4: Schematic exemplar of different stages of a heavy-ion collision, the *Little Bang*. The figure is taken from Ref. [26]

the space-time evolution of an AB collision in its CM frame is also schematically represented in Figure 1.5, in a light-cone (b) with and (a) without taking QGP formation into account. The beam (longitudinal) direction is plotted along the horizontal and proper time is plotted along the vertical axis. As the system is expanding under pressure gradients and cools down with evolving time, different stages of its space-time evolution are broadly classified in the following way.

- **Initial Stage**: Two nuclei approach each other with relativistic speed. Due to Lorentz contraction along the beam direction they look like pancakes. Conventionally, these two nuclei collide at $\tau = 0$ fm/c and produce a nuclear matter with non-uniform

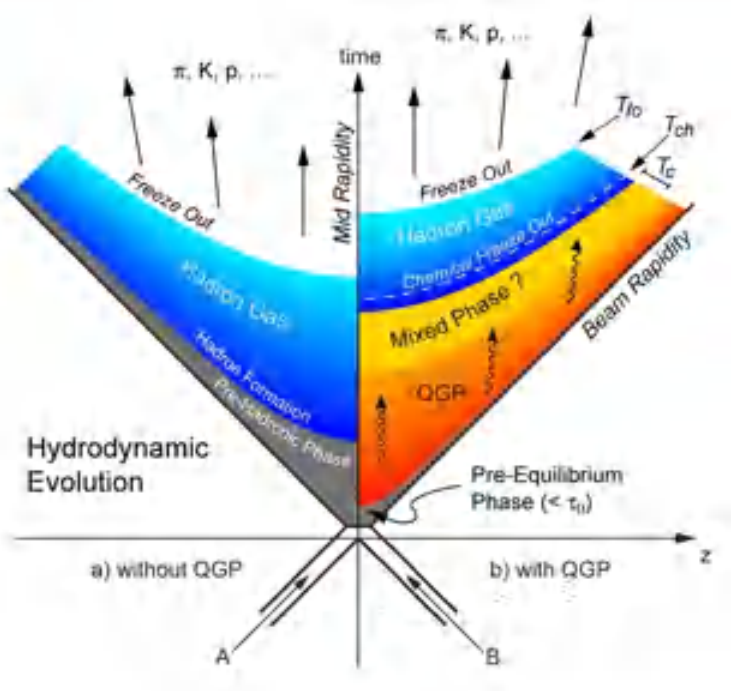

Figure 1.5: Space time evolution of a high-energy collision between two nuclei in their CM frame, (a) without and (b) with QGP formation. The figure is taken from Ref. [27].

energy density. This type of non-uniformity plays an important role in the final state flow measurements. The overlapping part of the colliding nuclei form an intermediate fireball. If sufficient amount of energy is available during the collision, the hadronic boundaries may melt down and partonic degrees of freedom are excited within the fireball. If not, then depending on the amount of stopping suffered by the colliding nuclei, the fireball is either dominated by mesons or rich in baryons. The system remains in a pre-equilibrium state for about $\lesssim$ 1 fm/c, and till date very little is understood about this stage of the collision.

- **Thermalization**: Due to multiple scattering between the constituent particles local thermal equillibrium is quickly achieved in the fireball within a time period of $\tau_0 =$ 1 fm/c, and remains in the equilibrated condition for a duration of $1 - 10$ fm/c. If partonic degrees of freedom are excited then after thermalization, the quarks and anti-antiquarks present in the thermalized matter follow Fermi-Dirac distribution, whereas the gluons follow Bose-Einstein distribution. Due to a pressure gradient that builds up during thermalization the fireball matter is then driven radially outward.

- **Hadronization**: The equilibrated fireball expands and cools down. When the temperature goes below a critical temperature (T_c) the quarks, antiquarks and gluons start to combine to form colorless bound states, a process known as hadronization. It is quite possible that for some time the fireball remains in a mixed state of QGP

and hadron gas. If on the other hand sufficient heating and/or compression is/are not achieved, the interacting nucleons will directly produce new particles, most of which are π-mesons. The process is known as multiparticle production and it takes about $20 - 50$ fm/c of time. How these particles are produced, still remains an unresolved issue, one has to depend mostly on speculative measures.

- **Hadron Gas**: As hadronization stops, the fireball system forms a Hadron Gas (HG). The newly produced hadrons are weakly coupled. However, the entire system is still in equilibrium because of the inelastic interactions taking place within it, and it exhibits a collective behavior. Moreover, the hadrons in the HG state have sufficient energy to exchange quarks and antiquarks among themselves. The lifetime of this state is small and hence it has limited influence on the evolution process [28]. However, both the equilibrium and HG stages are guided by viscous hydrodynamics.

- **Chemical freeze-out**: As the HG expands further, the temperature drops down, and as a result the inelastic interactions cease to take place. At this moment the hadrons stop exchanging quarks among themselves or in other words the relative abundance (chemical composition) of every hadron species becomes fixed. This is known as *chemical freezeout*.

- **Kinetic freeze-out**: The momentum exchange among the hadrons continues until the elastic interactions cease. When that happens a *kinetic freezeout* is achieved, and the momentum spectra of the produced hadrons remain unchanged hereafter, final state particles freely stream out from the collision zone. Studies related to the momenta spectra aids to extract the freeze-out temperature and radial flow velocity.

1.2.2 Thermodynamics of the fireball

E. Fermi first applied statistical mechanics to multiple meson production in high-energy collisions [29]. He assumed that when two nucleons collide they release their energies within a very small volume $V = 2m_N V_0/\sqrt{s_{NN}}$, where $V_0 = 4\pi R_\pi^3/3$ and $R_\pi = 1/m_\pi$ is the Lorentz contracted characteristic length associated with the pion field. A large number of particles are formed instantaneously. The mean free path of these particles is small compared to the dimension of the interaction volume, and a statistical equilibrium is set up. Subsequently the system decays into one of the many accessible multiparticle states. The decay probability is calculated in the framework of standard statistical physics. The main reason behind using statistical concepts was the large value of strong coupling constant that prohibits any application of perturbative methods. The transition probability from an initial to a given final state is proportional to the modulus square of the transition matrix element, treated as

a constant, and to the density of states. The main effect comes therefore from the available phase space, which grows with increasing collision energy. The probability of having an n-particle final state is proportional to,

$$S(n) \;=\; \left[\frac{V}{(2\pi)^3}\right]^{(n-1)} \frac{dN}{dE} \tag{1.7}$$

where dN/dE is the density of states. The power $(n-1)$ comes because only $(n-1)$ particles have independent momentum. Fermi argued that at very high energies even a detailed statistical description may not be necessary [29]. Assuming that the matter is thermalized, one can calculate the temperature of the produced hadronic system from thermodynamic considerations valid for massless particles as,

$$T^4 \;=\; \frac{3\,\varepsilon^2}{2\pi^2 V_0\, m_N} \;=\; \frac{9\varepsilon^2 m_\pi^3}{8\pi^3 m_N}$$

The above equation may be used to calculate the abundance of produced particles from the thermodynamic relations giving the particle densities in terms of temperature.

In the framework of MIT bag model we can construct a static idealization of the fireball system created in AB collisions [30, 31]. Complexities and finer details that are needed to describe a more realistic system can be gradually added on at later stages. In the bag model a hadron is considered as a spherical enclosure of radius R. Each quark and/or antiquark, a spin$-\frac{1}{2}$ fermion, is massless inside the bag but infinitely massive outside. Gluons on the other hand are massless spin-1 bosons. Due to the presence of quarks (anti-quarks) normal QCD vacuum is destroyed within the bag and a perturbative QCD vacuum prevails inside. Energy and momentum conservation at the bag surface is ensured by introducing an external (inward) pressure at the bag surface to balance the internal (outward) pressure of the confined quarks. This bag pressure is characterized by a constant B. The quark-gluon system can be treated as an ideal relativistic gas of massless ($\epsilon = pc$) particles at an equilibrium temperature T. The energy densities of the quarks, antiquarks and gluons can be derived by using the respective distribution formulae, and that for the QGP system (ε_{qgp}) by adding these energy densities together and combining the degeneracy factors [32–34],

$$\varepsilon_{qgp} \;=\; \varepsilon_q \;+\; \varepsilon_{\bar{q}} \;+\; \varepsilon_g \;=\; \left(\frac{37\pi^2}{30}\,T^4 \;+\; 3\mu_q^2\,T^2 \;+\; \frac{3\mu_q^4}{2\pi^2}\right) \tag{1.8}$$

Here $\mu_q = \mu_{\bar{q}}$ is the quark (anti-quark) chemical potential, $\varepsilon_q\,(\varepsilon_{\bar{q}})$ is the energy density of an ideal quark (ant-quark) gas and ε_g is the same for an ideal gluon gas. One expects a stable QGP when the pressure inside $P = \frac{1}{3}\varepsilon \geqslant B$, the equality holds at the boundary of stability. The condition may be used to arrive at the limiting critical values of the temperature T_c,

the chemical potential μ_c and the baryon number density n_c,

$$\begin{aligned} T_c\,(\mu_q = 0) &= \left(\frac{90B}{37\pi^2}\right)^{\frac{1}{4}} \approx 147\,\mathrm{MeV} \\ \mu_c\,(T = 0) &= \left(2\pi^2 B\right) = 0.43\ \mathrm{GeV} \\ n_c\,(T = 0) &= \frac{2}{3\pi^2}\left(2\pi^2 B\right)^{\frac{3}{4}} = 0.72\ \mathrm{fm}^{-3} \end{aligned} \tag{1.9}$$

If the quark – quark and quark – anti-quark interactions are taken into account, then the above expression of energy density is modified as [35],

$$\varepsilon = \left(\frac{37\pi^2}{30} - \frac{11\pi}{3}\alpha_s\right) T^4 + \left(1 - \frac{2}{\pi}\alpha_s\right) 3\mu_q^2 T^2 + \left(1 - \frac{2}{\pi}\alpha_s\right) \frac{3\mu_q^4}{2\pi^2} \tag{1.10}$$

Using the stability condition and setting the corresponding chemical potential μ_c and temperature T_c we get

$$B = \left(\frac{37\pi^2}{90} - \frac{11\pi}{9}\alpha_s\right) T_c^4 + \left(1 - \frac{2}{\pi}\alpha_s\right) {\mu_c}^2 T_c^2 + \left(1 - \frac{2}{\pi}\alpha_s\right) \frac{{\mu_c}^4}{2\pi^2} \tag{1.11}$$

Under the limiting conditions

$$T_c(\mu_q = 0) = \left[\frac{B}{\left(\frac{37\pi^2}{90} - \frac{11\pi}{9}\alpha_s\right)}\right]^{\frac{1}{4}} \quad \text{and} \quad \mu_c(T = 0) = \left[\frac{2\pi^2 B}{\left(1 - \frac{2}{\pi}\alpha_s\right)}\right]^{\frac{1}{4}} \tag{1.12}$$

Depending on the values of B and α_s chosen, the critical temperature T_c would lie somewhere between $150 - 200$ MeV and the chemical potential μ_c somewhere between $450 - 600$ MeV.

1.2.3 Hydrodynamics of the fireball

Relativistic hydrodynamics provides a simple picture of the space-time evolution of the hot and dense fireball matter produced in the central rapidity region (see Appendix A for details on rapidity) in a relativistic AB collision. It is assumed that the expanding system stays in local thermodynamic equilibrium. Without going into the details of any microscopic aspect, hydrodynamics allows us to describe all the stages of expansion of the fireball, starting possibly from the QGP, through hadronization and ending at the freeze out. Hydrodynamics, although classical in concept and formulation, provides an important computational tool to describe the gross features of AB collisions. It uses the fundamental conservation laws of energy and momentum to build an equation of state for the evolving system.

Landau's hydrodynamic model

Landau [36, 37] argued that one should not expect the number of finally emitted particles to be determined only from the equilibrium condition at the instant of collision. Rather the system continues interacting even after the initial stages and the number of particles becomes definite only when they are far apart in phase space. Landau too assumed that a compound system is formed, and energy is deposited in a small volume V, subjected to Lorentz contraction. In comparison with the dimension of the collision volume the mean free path of the produced particles is small, and a statistical equilibrium is set up. In the second stage of the collision, under the influence of a longitudinal velocity gradient the system starts expanding. The transverse gradients are also present, but initially the longitudinal gradient is predominant and the early expansion is approximated as one-dimensional. The expanding system is regarded as an ideal fluid with zero viscosity and zero thermal conductivity. During the expansion velocities of the particles are comparable to that of the light, justifying thereby the use of relativistic hydrodynamics. Particles are formed and absorbed in the system throughout the first and second stages of the collision. As the system expands, the mean free path of the particles becomes comparable to the dimension of the colliding system, and the interaction between the particles becomes weak. The expanding system then breaks up into individual particles when its temperature $T \sim m_\pi$. For a perfect fluid only one equation of state is necessary to describe the hydrodynamic expansion. A perfect fluid does not have any viscosity and during the hydrodynamic expansion the total entropy ($S = sV$) of the system remains unchanged. The number of pions produced was derived as,

$$N_\pi \propto sV \propto E_{cm}^{3/2} V/\gamma_{cm} \propto A E_{cm}^{1/2} \propto A E_{lab}^{1/4}$$

which implies that heavy nuclei are better suited for pion production and that pion multiplicity grows slowly with collision energy. Landau solved the hydrodynamic equations in one and three-dimensions. An exact solution was obtained in one-dimension [38] which gave the same result as Landau's in the asymptotic region. A necessary condition for the applicability of Landau's picture to central relativistic AB collisions is that, the nucleons in the front part of each colliding nuclei, while traversing through the other nucleus, must loose all of their kinetic energies in the center of mass frame. This demands that the average energy loss of these nucleons per unit length should be greater than a critical value given by,

$$\left|\frac{dE}{dz}\right|_{cr} = \frac{E_{cm}/2}{(2R/\gamma_{cm})} \tag{1.13}$$

Although at low energies ($E_{cm} < 10$ GeV) Landau's theory gives satisfactory results, but at ultra-relativistic energies ($E_{cm} = 200$ GeV) the above condition becomes too stringent to be attained. Hence, Landau's picture breaks down when the required stopping power

becomes too large. Furthermore, in contrast to the requirements of Fermi's and/or Landau's approach, the thickness of the colliding nuclei cannot be infinitely small even in the ultra-relativistic region. Also, in this model the boundary condition is specified at the time of maximum compression, whereas the entire matter is distributed over a small but finite volume. However, particle production is not an instantaneous process and it shows the characteristics of space-time correlation, i.e., fast particles are produced later and further away from the collision center than the slow particles, which is not considered in Landau's model. The main criticism of Landau's model is that, the leading particle effect is neglected. In order to achieve full stopping, removal of the radiation energy due to deceleration is required, which is also not taken into account. These difficulties can be removed if one assumes that during the collision, the valence quarks should move without much interaction and the energy carried by the gluon fields is stopped within the collision volume [39–41]. Such an assumption is justified because, due to the color degeneracy gluon-gluon interaction cross-section is larger than the quark-quark cross-section. To be consistent with the initial conditions of Landau's model the gluon field should thermalize after a certain time.

Bjorken's hydrodynamical model

Based on the assumption that at sufficiently high-energy the rapidity distribution of the final state particles is uniform in the mid-rapidity region, Bjorken introduced a hydrodynamic model [42] of AB collision. It is also assumed that the strongly interacting matter present within the collision volume, reaches a state of local thermal equilibrium after the collision and then expands adiabatically. The evolution of the system is determined by the initial conditions and an equation of state (EoS) that transfers the energy and baryon density to the pressure exerted by the system. The EoS is subjected to the constraints of local conservation of energy-momentum and currents [43, 44]. The EoS for a non-dissipative ideal fluid can be mathematically formulated as,

$$\begin{aligned} \partial_\mu T^{\mu\nu}(x) &= \partial_\mu[\{\varepsilon(x) + P(x)\}u^\mu u^\nu - g^{\mu\nu}P(x)] = 0 \\ \partial_\mu j^\mu_B(x) &= \partial_\mu\left[n_B(x)u^\mu(x)\right] = 0 \end{aligned} \tag{1.14}$$

where

$$T^{\mu\nu} = [\varepsilon + P]\; u^\mu\, u^\nu - g^{\mu\nu}\, P$$

is the relativistic stress energy tensor, ε is the energy density, P is the pressure, j^μ_B is the charge-current density, n_B is the baryon number density and $u^\mu = (\gamma, \gamma\,\bar{v})$ is the four-velocity, all defined in the local rest frame (x) of the fluid. In Bjorken's theory all thermodynamic quantities characterizing the central region should depend only on the longitudinal proper time $\tau = \sqrt{t^2 - z^2}$ and longitudinal velocity $u_z = z/t = \tanh y$, so that

$u^\mu = (t/\tau,\, 0,\, 0,\, z/\tau)$. Under the above condition Bjorken's equation can be written as,

$$\frac{\partial \varepsilon}{\partial \tau} + \frac{\varepsilon + P}{\tau} = 0 \tag{1.15}$$

Using $\varepsilon = \lambda P$ where $\lambda = dP/d\varepsilon$ measures the elastic wave velocity in the medium, and the thermodynamic relation: $\varepsilon + P = Ts + \mu_{_B} n_{_B}$, we get

$$\varepsilon(\tau_f) = \varepsilon(\tau_i) \left(\frac{\tau_i}{\tau_f}\right)^{1+\lambda} \tag{1.16}$$

For a zero baryon density

$$s(\tau_f) = s(\tau_i) \left(\frac{\tau_i}{\tau_f}\right) \quad \text{and} \quad T(\tau_f) = T(\tau_i) \left(\frac{\tau_i}{\tau_f}\right)^{\lambda} \tag{1.17}$$

A QGP to HG phase transition causes softening of the EoS. As the temperature crosses its critical value, the energy and entropy densities quickly increase while the pressure rises slowly. The derivative $dP/d\varepsilon$ has a minimum at the end of the mixed phase, known as the softest point. The diminishing driving force slows down the build-up of flow. The preliminary conditions which are the input parameters, define the initiation of the hydrodynamic evolution and the relevant macroscopic density distributions at that point of time. The hydrodynamic evolution is terminated by implementing the freeze out condition, which describes the breakdown of local equilibrium due to decreasing local thermalization rates. In non-central collisions, driven by its inner asymmetric pressure gradients, the system will expand more prominently in the direction of the reaction plane than in the direction perpendicular to the reaction plane. As the time evolves, the system becomes less and less deformed. To estimate the initial energy density of a Bjorken-type fluid element, one has to go to the fluid rest frame. All particles are originating from a cylindrical volume of cross-section A, which actually is the overlap area of the interacting nuclei, and of length $v_z t$. We concentrate on a thin slab of thickness dz centered between the two pancake-like moving nuclei. The point of impact is assumed to be the origin ($z = 0$) of our frame of reference. Therefore $dz = \tau \cosh y\, dy$ and we may ignore the collisions among produced hadrons. The energy density is obtained as,

$$\varepsilon_{BJ} = \frac{\Delta E}{\Delta V} = \frac{E}{A}\frac{dN}{dz} = \frac{m_t}{\pi R^2 \tau}\frac{dN}{dy} = \frac{1}{\pi R^2 \tau}\frac{dE_t}{dy} \tag{1.18}$$

Taking the proper time $\tau \approx 1$ fm/c and dN/dy to be the central rapidity density of produced particles, this relation was first derived by Bjorken [42]. However, a perfect fluid must undergo an isentropic expansion. In order to compensate the Lorentz contraction, a relation like $s_i\, \tau_i = s_f\, \tau_f$ should hold between the initial and final proper time. If we consider

massless particles, then $\varepsilon \propto T^4$ and $s \propto T^3$. Correspondingly,

$$\varepsilon_f = \varepsilon_i \left(\frac{\tau_i}{\tau_f}\right)^{4/3} \tag{1.19}$$

which contradicts Bjorken's formula, $\varepsilon_{BJ} \sim \tau^{-1}$. The energy density formula should therefore be modified as,

$$\varepsilon = \frac{1}{\pi R^2 \tau_0} \frac{dE_t}{dy} \left(\frac{\tau_f}{\tau_i}\right)^{1/3} = 2\,\varepsilon_{BJ} \tag{1.20}$$

1.2.4 QCD phase diagram

The QCD phase diagram serves as a very useful summary of the properties of a many-body system of strongly interacting particles. These properties, analogous to condensed matter physics, are mostly thermodynamic in nature, and they describe the collective behavior of a system of many particles responding to a few external control parameters like the temperature (T) and baryochemical potential ($\mu_{_B}$). Using some general arguments arising from QCD, experimental observation and common sense, we may try to explain qualitatively some of the features depicted in the QCD phase diagram [Figure 1.6]. Quantitative details like the order of phase transition and corresponding values of control parameters, suffer from large uncertainties. Since it was first introduced [13] the phase diagram has seen quite a few changes, as new phases of QCD matter find out their places in it and new lines are being drawn to demark one phase from another. In the bottom left-hand corner of the phase diagram, where T and $\mu_{_B}$ are both very small, the thermodynamic behavior of QCD matter can be described in terms of a hadron gas. The many-body phase at these low temperatures and densities behaves more like a vapor because the force between color-neutral hadrons is a very weak second-order effect similar to the Van der Waal's force between neutral atoms. Two regimes are of particular interest to us, (i) $T \to \infty,\ \mu_{_B} = 0$, along the y-axis and (ii) $T = 0,\ \mu_{_B} \to \infty$, along the x-axis of Figure 1.6. Keeping $\mu_{_B}$ fixed at zero if we increase T, lattice calculations indicate that at a critical temperature $T_c \sim 150$ MeV the hadron gas must undergo a phase transition to a deconfined colored soup of quarks and gluons [45]. The process is similar to the ionization of atoms in a QED plasma at high temperature. An important order parameter for this phase transition is the chiral quark condensate $\langle q\bar{q}\rangle$. The nature of this transition is very sensitive to the values of quark masses. If up and down quarks are massless and the rest are infinitely massive then in QCD the transition is of second order [46]. If up, down and strange quarks are massless then the transition is of first order [47]. For realistic quark masses lattice calculations at $\mu_{_B} = 0$ show that the HG to QGP transition is a smooth but rapid cross-over [48–50]. It should be noted that the early universe evolved from a high temperature big bang epoch, and in the process of cooling

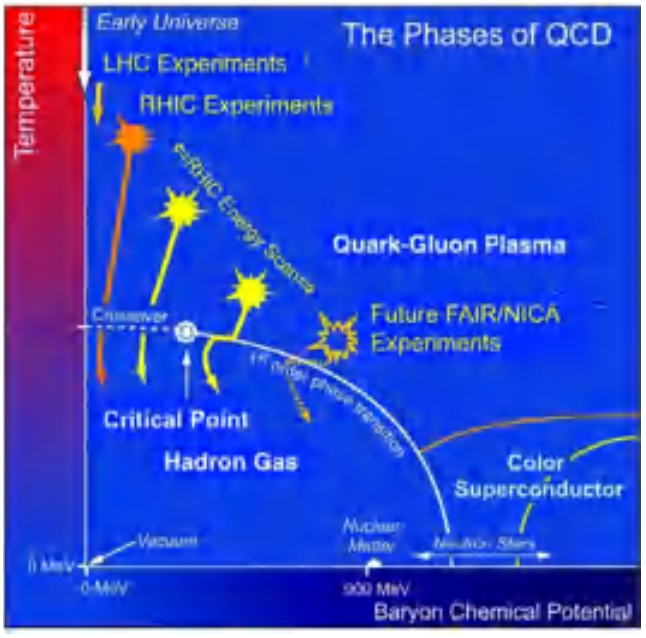

Figure 1.6: A schematic of the QCD phase diagram showing locations of different states of hadronic/partonic matter [51].

it presumably underwent the reverse phase transition from a primordial QGP into a HG. Although this regime is net baryon-free, it is still a high matter density at high temperature environment, since the energy density is sufficient to cause rapid production of $q\bar{q}$ pairs and gluons. Such an extended QCD state, strongly interacting, has perhaps already been created in the RHIC and LHC experiments on heavy-ion interactions. Along the x-axis of Figure 1.6 the dynamics however is quite different. In this region the net baryon density $\rho_{_B}$, measured by its conjugate the net baryo-chemical potential $\mu_{_B}$, can be a good order parameter. As the chemical potential is increased, initially there is no change. Because at zero temperature the chemical potential $\mu_{_B}$ is the energy required to add a baryon to the system, and QCD has a large mass gap for baryonic states. The first non-vacuum state one encounters along the $\mu_{_B}$-axis of the phase diagram is the nuclear matter, a strongly correlated superfluid composed of non-relativistic neutrons and protons. The baryon density changes discontinuously at the onset transition, from $\rho_{_B} = 0$ to the nuclear matter density $\rho_{_N} = 0.16$ fm^{-3}. The discontinuity decreases as nuclear matter is heated, and the nuclear liquid-gas phase transition ends at a critical point $T \approx 18$ MeV [52]. For T slightly above zero, continuity ensures that the transition remains of first order, as probed in the nuclear multi-fragmentation processes [53]. As $\mu_{_B}$ is increased further, the utility of $\rho_{_B}$ as an order parameter is lost, as it is only expected to increase monotonically. We have to revert back to $\langle q\bar{q}\rangle$ as the signal for chiral symmetry restoration. At $\mu_{_B} \gtrsim 1$ GeV, corresponding to matter densities $\sim 5-10$ times the nuclear matter density, in a completely Fermi-degenerate sea of quarks chiral symmetry is expected to be restored. Various theoretical studies indicate that the phase transition in this region is of first order. For slight temperature perturbations

in this Fermi-degenerate chirally symmetric phase, interesting dynamics like quark-quark pairing on the Fermi-surface is expected, leading to the remarkable Cooper pair-like color superconductive states. For our purpose, it is sufficient to note that, since on the x-axis we have a first order phase transition and along the y-axis there is a smooth crossover, by continuity it follows that the mutation from first order transition to cross-over should be marked by a critical end point (CEP). The CEP is interesting because it is the only thermodynamically stable point on the phase transition line at which the correlation length diverges. This means that the CEP may manifest itself in heavy-ion collisions in terms of enhanced fluctuations of dynamically and intrinsically conserved quantities. The CEP is indicated in Figure 1.6 and its exact location is a subject of current theoretical and experimental studies.

In the ideal version of QCD the quarks are considered as massless objects. The left and right-handed quarks are decoupled from each other, corresponding quark currents are separately conserved and QCD Lagrangian is invariant under their interchange. Hadrons on the other hand, have well defined parities and for them no parity partners are observed. This paradox is resolved by a phenomenon called the spontaneous breakdown of chiral symmetry. The quarks inside a nucleon/hadron polarize the surrounding gluonic medium. The resulting gluon cloud around each quark provides it with a dynamically generated effective mass, which results in a spontaneous breaking of the chiral symmetry of the QCD Lagrangian. One would expect that this symmetry is restored at high energies where quarks and gluons are the correct degrees of freedom. As mentioned above, in high-energy heavy-ion collisions it is possible to sufficiently heat up and/or squeeze the nucleonic matter, so that the boundaries of individual hadrons/nucleons melt down, color-neutral states are dissolved, producing a medium of color-charged constituents. The deconfinement transition thus becomes the QCD counterpart of the insulator-conductor transition of atomic physics [54]. Hadronic matter thus shows two transitions, deconfinement and chiral symmetry restoration. Some general arguments suggest that they either occur at the same point or, deconfinement precedes the chiral symmetry restoration. It is quite possible that quarks, as they become deconfined, can maintain their effective mass up to some higher temperature or density. Lattice calculations have shown that for vanishing baryon density, deconfinement and chiral symmetry restoration do in fact coincide, indicating that the deconfinement temperature is sufficient to melt the effective quark mass. For high baryon density at low temperature, this however seems unlikely. In addition to the hadronic matter and plasma of deconfined massless quarks and gluons, an additional state of massive quarks is very much possible. We note that in particular the anti-triplet quark-quark interaction provides an attractive force, making it possible that diquarks as localized bound states exist. Such colored bosonic states can condense and therefore form a color superconductor as yet another state of strongly interacting matter.

1.3 Signatures of QGP signal : Experimental observables

A QGP state created in high-energy heavy-ion collisions should be extremely hot, dense, short lived, and it would not be directly accessible to the experiments. One can detect only the final state particles, freely streaming out from the reaction zone that went through the hadronization process. However, these particles and their distributions are quite useful to trace back the properties of fireball medium in terms of such observables that are almost insensitive to the process of hadronization. Here we are going to discuss some such experimental signatures of the QGP.

1.3.1 Charmonium suppression

J/ψ is a bound state of charm quark pairs ($c\bar{c}$). QCD calculations predict that J/ψ production should be suppressed in a QGP medium [55]. J/ψ is produced mostly at the initial stages of the collision through hard and pre-thermal processes. In a QGP medium the charm and anti-charm quarks do not bind to form hadrons while passing through the deconfined matter, instead they just move apart from each other. Due to the heavy mass associated with the charm quarks the production of $c\,(\bar{c})$ is also limited during hadronization. It is the quarks and gluons of the deconfined matter that screen the strong potential of the c and $\bar{c}$ quarks. This is similar to the Debye screening of QED, which prevents them from binding together and form a J/ψ. The phenomenon can be understood as following.

The inter-quark potential is given by Equation (1.2). The parton density around c and $\bar{c}$ gets modified due to Debye screening of color charges between c and $\bar{c}$. This in turn modifies the inter-quark potential to,

$$V(r) = -\frac{g\,\exp\left(-r/r_D\right)}{4\pi\, r} \tag{1.21}$$

where r_D is the Debye screening length. According to perturbative QCD estimation, r_D should be inversely proportional to the temperature of the QGP phase. At high temperature r_D becomes smaller. As a consequence the range of attractive potential in Equation (1.21) becomes smaller. Therefore, at extreme temperatures it would be impossible for $c\bar{c}$ pairs to form bound states. The separated c and $\bar{c}$ quarks in the deconfined phase would rather hadronize by combining with other light quarks present in the system. In comparison with pp collisions where formation of QGP is not expected, the J/ψ yield will be suppressed in AB collisions where QGP is expected to form. To quantify the extent of J/ψ suppression a nuclear modification factor is introduced as,

$$R_{AA}^{J/\psi} = \frac{\frac{1}{N_{ev}}\frac{d^2N_{J/\psi}}{dp_T\,dy}\big|_{\rm cent}}{\langle T_{AA}\rangle\frac{d^2\sigma_{J/\psi}}{dp_T\,dy}|_{pp}}$$

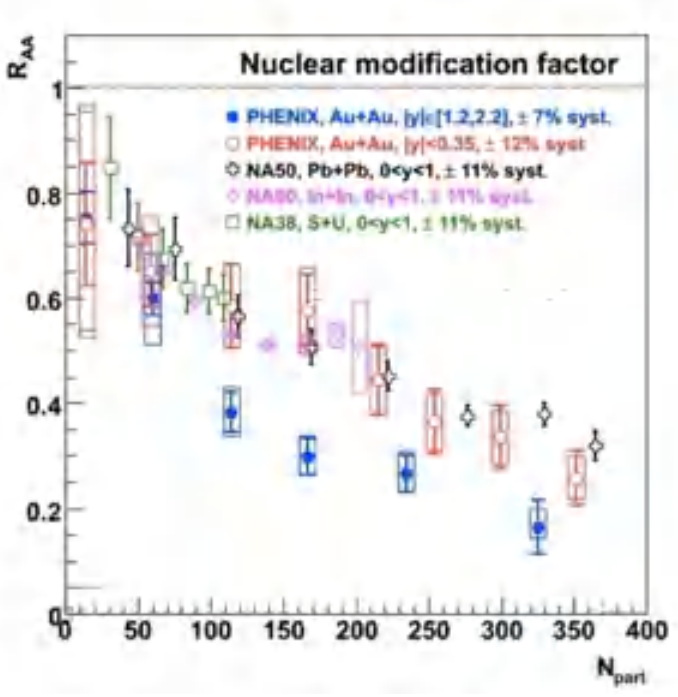

Figure 1.7: Centrality dependence of J/ψ R_{AA}. This figure is taken from Ref. [56].

Here $N_{J/\psi}$ is the J/ψ yield per centrality in AA collisions, $\langle T_{AA} \rangle$ is the average nuclear overlap function per centrality in AA collisions, and $\sigma_{J/\psi}$ is the J/ψ cross-section in pp collisions. N_{ev} is the number of AA events within a particular centrality class. $R_{AA}^{J/\psi}$ as a function of $N_{\rm part}$ is shown is Figure 1.7 for a wide range of energies from SPS [57, 58] to RHIC [59]. If the value of R_{AA} is less than unity, it is a manifestation of the suppression, which in turn is an evidence of a quark-gluon medium created in heavy-ion collisions.

1.3.2 Jet quenching

Jet is a group of high energy particles which are highly correlated in their direction. In AB collisions partons are produced due to hard processes. Fragmentation of these partons while escaping the collision zone results in production of jets. Figure 1.8 shows the schematic of a di-jet, a pair of jets moving in opposite directions. If a di-jet is produced near the surface of the fireball, then the near side jet will propagate normally, while the away side (opposite to the nearby fireball surface) jet will be smeared out. The smearing effect is ascribed to the fact that the away side jet passes through a longer distance in the hot and dense medium, suffering multiple interactions with the partons present therein. As a consequence its momentum will be lost and the phenomenon is known as *jet quenching* [60, 61]. The effect was first noted at RHIC [62] while investigating the two particle azimuthal correlation. It is observed from Figure 1.8 that in Au+Au collision the away side ($\Delta\varphi = \pi$) jet disappears,

whereas the same is present in d+Au and p+p collisions. Thus, jet quenching can be considered as an unambiguous signature of the QGP formation in AB collisions. Another approach to examine the jet-medium interaction is the measurement of nuclear modification factor (R_{AA}) for an inclusive jet production, which is defined as,

$$R_{AA}^{jet} = \frac{\frac{1}{N_{ev}} \frac{d^2 N_{jet}}{dp_T\, dy}|_{\text{cent}}}{\langle T_{AA} \rangle \frac{d^2 \sigma_{jet}}{dp_T\, dy}|_{pp}}$$

where the symbols have similar meaning as described in 1.3.1 with J/ψ being replaced by 'jet'. Figure 1.9 shows a clear indication of jet suppression at a LHC energy relative to the pp collision. Jet quenching is maximum for the most central collisions, decreases monotonically from central to peripheral events, which again confirms the formation of a dense partonic

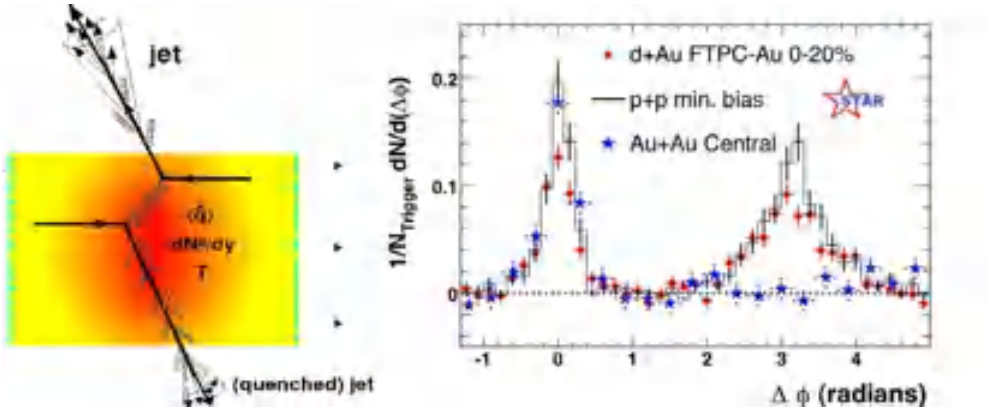

Figure 1.8: Left: Schematic of di-jet production. Right: Distribution of azimuthal angle difference between trigger and associated particles at STAR from central Au+Au, d+Au, and p+p collisions. The figure is taken from Ref. [62].

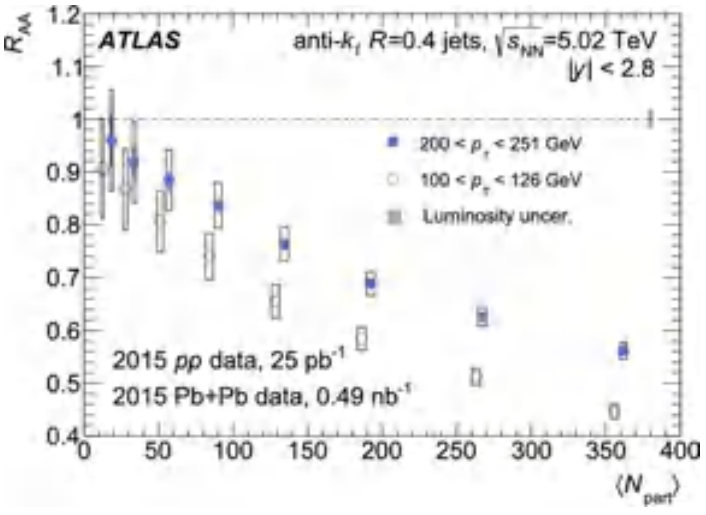

Figure 1.9: R_{AA} values for jets considering two different p_T intervals at midrapidity as a function of N_{part}. The figure is taken from Ref. [63].

medium in central collisions. Jet quenching is also observed to decrease (increase in R_{AA}) with increasing jet-p_T at almost all centrality classes for which $N_{\text{part}} \geq 50$. Below $N_{\text{part}} = 50$ the differences are not statistically significant.

1.3.3 Strangeness enhancement

Unlike the u and d quarks, the strange (s) quarks are not present in the colliding nuclei. Thus, any detection of a strange particle is attributed to a s-quark formation using the kinetic energy of the colliding system. Strangeness production is believed to be a key observable having the potential to deliver an in-depth information on the reaction dynamics of AB collisions [64, 65]. It should be noted that strangeness disappears only through weak

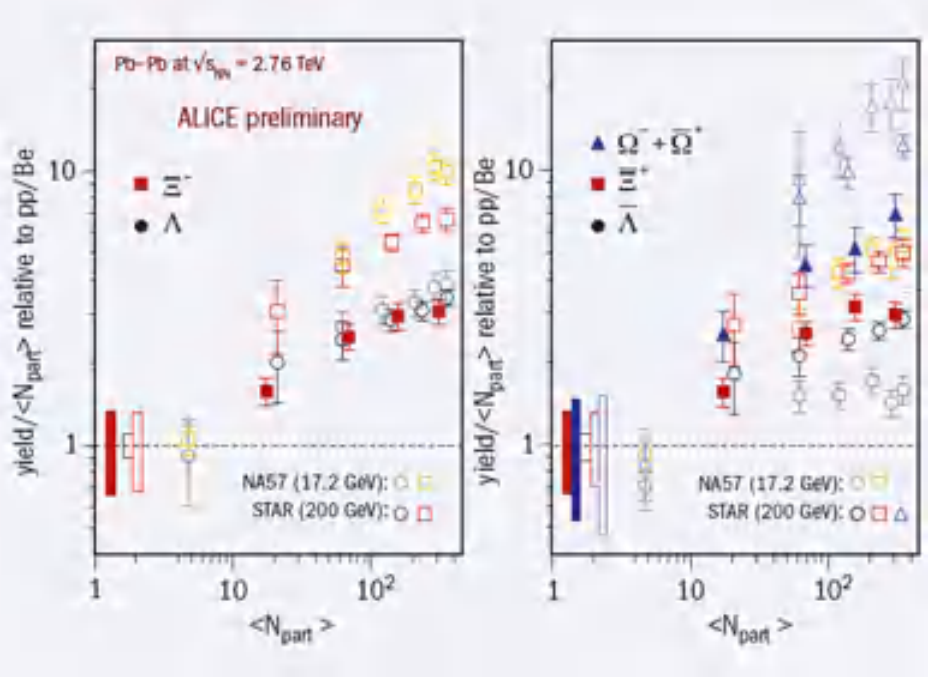

Figure 1.10: Strangeness enhancements at midrapidity as a function of N_{part}, showing LHC, RHIC and SPS data simultaneously. The figure is taken from Ref. [66].

decay. This decay mode being a longer process than hadronization, strange hadrons can survive hadronization and can bring out undistorted information about the initial stages of the fireball system. Coupling of gluons, $g+g \rightarrow \bar{s}+s$ is the dominating process of strangeness production in a QGP phase. These interactions occur very rapidly and s-quark abundance is equilibrated in plasma. Strangeness enhancement in dense baryonic matter may be a consequence of Pauli's exclusion principle. Strangeness enhancement is measured in terms of its enhancement factor defined as the yield per participating nucleons of a particular type of strange particle in AB collisions relative to the strange particle yield in a reference system like say, pp collisions. Figure 1.10 shows the strangeness enhancement as a function

of centrality observed at midrapidity for various species of particles in SPS [67], RHIC [68] and LHC [66] energies. Strangeness enhancement is noticed to increase with centrality and also with the strangeness content.

1.3.4 Electromagnetic probes

Photons associated with different amounts of momentum transfer are produced during the entire lifetime of the fireball formed in heavy-ion collisions. Photons do not interact strongly and in addition their mean free path is so large in comparison to the system size, that they suffer almost no collision in the medium before reaching the detectors. In other words, photons can bring out undistorted information from their time of production. Different processes of photon production from the instant of collision to freeze-out can be summarized as following:

1. The hard parton-parton scattering during the first stage of the collision gives rise to prompt photons. These photons are expected to be produced isotropically. The rate of their production decreases as an inverse power of p_T and increases with energy.

2. Next is the QGP phase where the dominating process of photon production are:
   (i) Annihilation – this is generally a quark-antiquark interaction like, $q + \bar{q} \rightarrow \gamma + g$ and $q + \bar{q} \rightarrow \gamma + \gamma$. The probability of occurence of the second process is smaller by a factor of $\alpha_e/\alpha_s \approx 0.02$ and usually not considered.
   (ii) Compton process – in this process a gluon interact with a quark and produce a quark and photon like, $g + q \rightarrow q + \gamma$ and $g + \bar{q} \rightarrow \bar{q} + \gamma$. These *thermal* photons help to investigate the thermodynamic properties of the fireball medium.

3. As the system expands and cools down, hadronization follows the QGP state. Photons produced during hadronization are labeled as *hadron gas* photons which are produced from resonance decays and scattering of π, ρ, ω, and others. Most common contribution to the photons in this stage are from the following schemes: $\pi^+ + \pi^- \rightarrow \gamma + \rho^0$ and $\pi^\pm + \rho^0 \rightarrow \gamma + \pi^\pm$.

4. Additional photons may also originate from hadronic decays after freeze out by $\pi^0 \rightarrow \gamma + \gamma$, $\eta \rightarrow \gamma + \gamma$, and higher resonances.

The direct photons (thermal and hadron gas) produced in phase 2 and 3 provide some idea about the degree of thermalization of the fireball. The rapidity distribution of these photons unveil the initial rapidity of the produced mesons or directly the QGP [69]. However, it should be noted that it is extremely difficult to extract these direct photons from the

huge background produced from the prompt photons and also hadronic decays of π^0 and η. The contribution from direct photons in heavy-ion collisions is estimated by obtaining the direct photon distribution in *pp* collisions and then scaling the yield with number of binary collisions. On the other hand, the contribution from aforementioned hadronic decays are experimentally removed using the invariant mass reconstruction technique.

1.3.5 Collective flow

The major focus of this thesis is on collective flow analysis and allied effects of charged hadrons. In this context we are going to provide a review with a little more details than the other signatures described above, on some results pertaining to the collective flow of hadronic matters available from different experimental facilities like AGS, SPS, RHIC, and LHC. With reference to heavy-ion collisions collectivity refers to some common properties exhibited by the emitted particles. There may be emission of many hadrons with a common velocity or in a common direction or even ejection of many particles of similar type. There are many underlying collective phenomena related to the common feature of the final state particles that can be broadly classified in the following manner.

- *Longitudinal flow* illustrates the collective behavior of the particles along the beam direction.
- *Radial flow* describes the motion of particles emitted from the source with a common velocity independent of the direction. This type of flow is mainly observed in central collisions where the system is azimuthally almost symmetric.
- An enhanced emission of particles along the direction of orientation of the impact parameter vector is termed as the *directed flow* or *side flow*.
- *Anisotropic flow* or particularly the *elliptic flow* refers to the non-uniform azimuthal distribution of particles where the final state have some azimuthal preference with back to back symmetry.

Ollitrault in 1992 for the first time predicted that "anisotropies in transverse-momentum distributions [will] provide an unambiguous signature of transverse collective flow in ultra-relativistic nucleus-nucleus collisions" [70]. Different equations of state and initial conditions were incorporated in his ideal hydrodynamic calculations to quantify this effect. In non-central collisions, the initial spatial anisotropy of the fireball, which is generally of almond shape, through multiple (re)scatterings among the particles is converted to a final momentum space anisotropy. A pictorial representation of the effect is depicted in Figure 1.11.

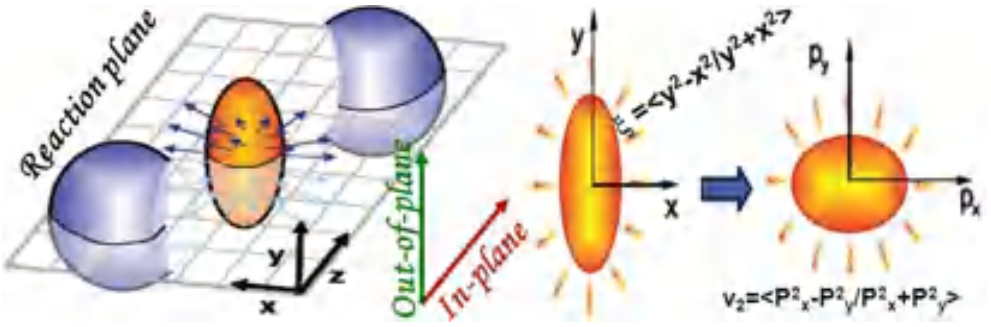

Figure 1.11: Schematic of initial space anisotropy w.r.t the reaction $(x-z)$ plane being converted into momentum space anisotropy due to in-medium interactions among the final state hadrons.

As the fireball system expands and cools down this anisotropy decreases, i.e. the system becomes more spherical. As a consequence there is a self quenching of the driving force. So, a scrutiny of the anisotropic flow will be sensitive to the dynamics that determines the early stage evolution of the collision [71]. It should be understood that in absence of strongly interacting matter, the distribution of the produced particles will be uniform on the transverse plane, thus anisotropic flow is a strong signature of presence of QGP. In order to understand different transverse flow effects, Voloshin and Poskanzer suggested a Fourier analysis of the azimuthal distribution of produced hadrons w.r.t to the reaction plane, a plane spanned by the beam axis and the impact parameter vector [72, 73]. This is generally expressed as,

$$E\frac{d^3N}{dp^3} = \frac{d^3N}{d\mathbf{p_T}dy} = \frac{d^2N}{2\pi p_T dp_T dy}\left[1 + 2v_1\cos(\phi - \Psi_{RP}) + 2v_2\cos 2(\phi - \Psi_{RP}) + ...\right] \quad (1.22)$$

where ϕ is the azimuthal angle of a produced particle and Ψ_{RP} is the reaction plane angle defined as the angle between the reaction plane and the x-axis of the laboratory system. v_n is the Fourier coefficient associated with the n-th harmonic. The flow harmonics are usually given by,

$$v_n = \langle\langle \cos n(\phi - \Psi_{RP})\rangle\rangle \quad (1.23)$$

where $\langle\langle\ \rangle\rangle$ denotes averaging over events and particles within a selected kinematic region. The first harmonic v_1 is called the *directed flow* parameter, which implies a preferential direction of particle emission either parallel ($v_1 > 0$) or anti-parallel ($v_1 < 0$) to the beam direction. Voloshin first coined the term *elliptic flow* to the 2nd harmonic (v_2). It is to be noted that the scenario of elliptic anisotropy changes from lower to higher energies for the colliding beams. At low energies the elliptic shape of the particle transverse momentum distribution is elongated along a direction perpendicular to the reaction plane. This is due to the shadowing by the spectator nucleons due to which particle production in the reaction plane is blocked. This is referred to as squeeze-out or out-of-plane flow. It corresponds to

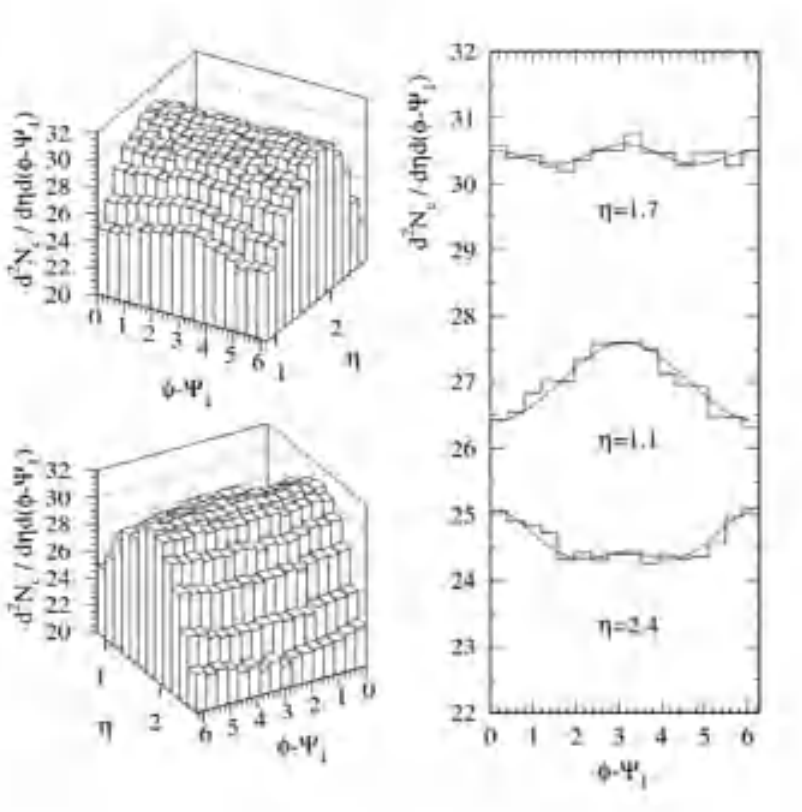

Figure 1.12: First measurement of in-plane elliptic flow by the E877 Collaboration at 11.8A Gev [74]. The solid line is a distribution with Fourier coefficients v_0, v_1, v_2 at three different pseudorapidity.

a negative value of v_2 and there is a preferential emission around $\Delta\phi = \frac{\pi}{2}$ and $\Delta\phi = \frac{3\pi}{2}$. The squeeze-out effect has got a special importance in AB collisions in the sense that any flow of nuclear/hadronic matter out of the reaction plane might escape the rescattering with the target and projectile spectators, thereby keeping the information of the interaction zone unaffected by the vigor of the collision. At higher energies the longitudinal size of the Lorentz contracted nuclei becomes negligible compared to its transverse size. In addition, the passing time of the nuclei becomes very small in comparison to the time required for development of elliptic flow. These factors interplay in such a manner that the shadowing is washed out and an in-plane elliptic flow develops. Now, there is a preferential emission at around $\Delta\phi = 0$ and $\Delta\phi = \pi$ which corresponds to positive v_2 values. In-plane elliptic flow was first observed at the AGS by the E877 Collaboration [74] as depicted in Figure 1.12. Later in the low energy scan at the AGS the E895 Collaboration [75] reported elliptic flow in the transition region from an out-of-plane to in-plane flow. However, at very low energies the picture is completely different, where the major effect is from the nuclei bouncing off from each other and then their fragmentation. These observations can be confirmed from Figure 1.13, where the p_T-integrated elliptic flow at midrapidity in the $20-30\%$ centrality bin is compared from measurements at lower energies to the LHC range. Integreted v_2 increases

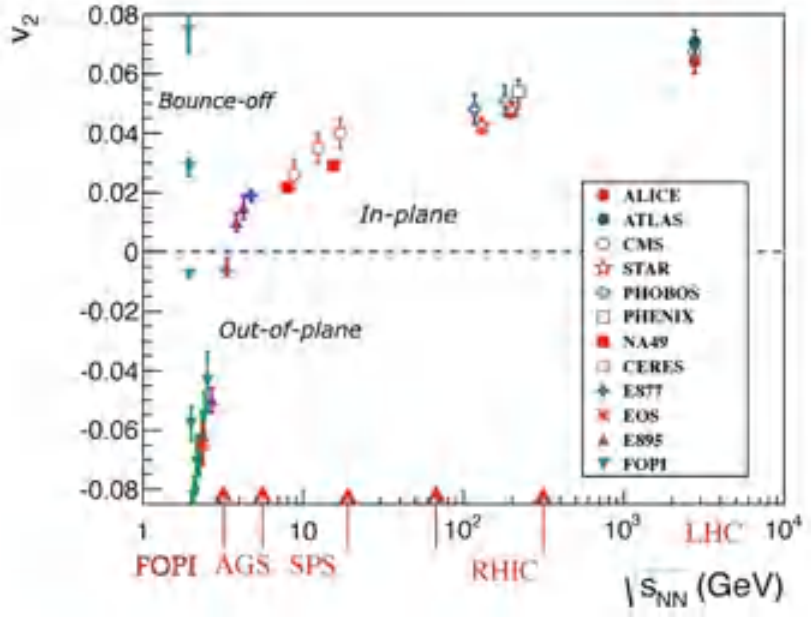

Figure 1.13: Elliptic flow at midrapidity in $20-30\%$ centrality bin as a function of energy from FOPI, AGS, SPS, RHIC to LHC. The basic figure is taken from [76] except certain textual changes.

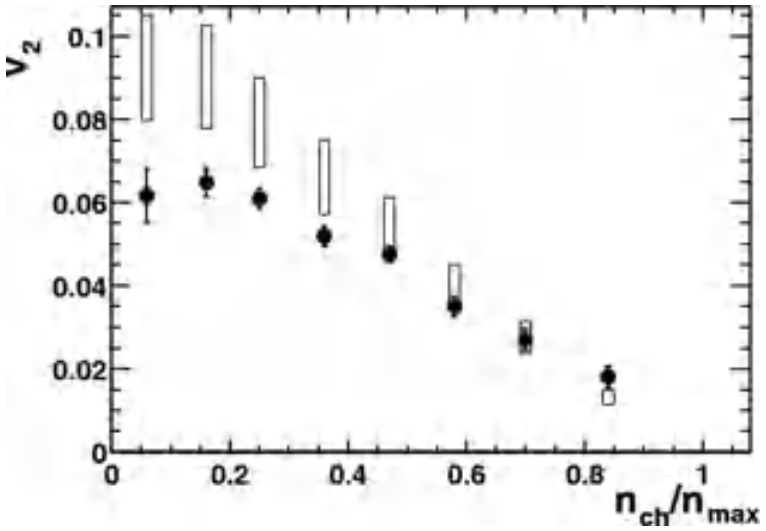

Figure 1.14: Elliptic flow as a function of centrality defined as $n_{ch}/n_{\max}$ reported by STAR Collaboration at $\sqrt{s_{NN}} = 130$ GeV [77]. The open rectangles show a range of values expected for v_2 in the hydrodynamic limit, scaled from ε, the initial space eccentricity of the overlap region.

by 30% from RHIC $\sqrt{s_{NN}} = 200$ GeV to LHC $\sqrt{s_{NN}} = 2.76$ TeV. The first measurement of v_2 at RHIC [77] is shown in Figure 1.14. The open rectangles are prediction of v_2 from hydrodynamic calculations. It is observed that the RHIC data agrees well with ideal hydrodynamics for $n_{ch}/n_{max} \geq 0.5$. This observation is an evidence of rapid thermalization of the system. The first results on elliptic flow at LHC energy [78] reported by the ALICE

collaboration is presented in Figure 1.15 and also compared with measurements at RHIC as obtained from STAR, shown by the solid lines. The elliptic flow at LHC follows the same trend as in RHIC but is higher in magnitude at same centrality. Elliptic flow coefficient

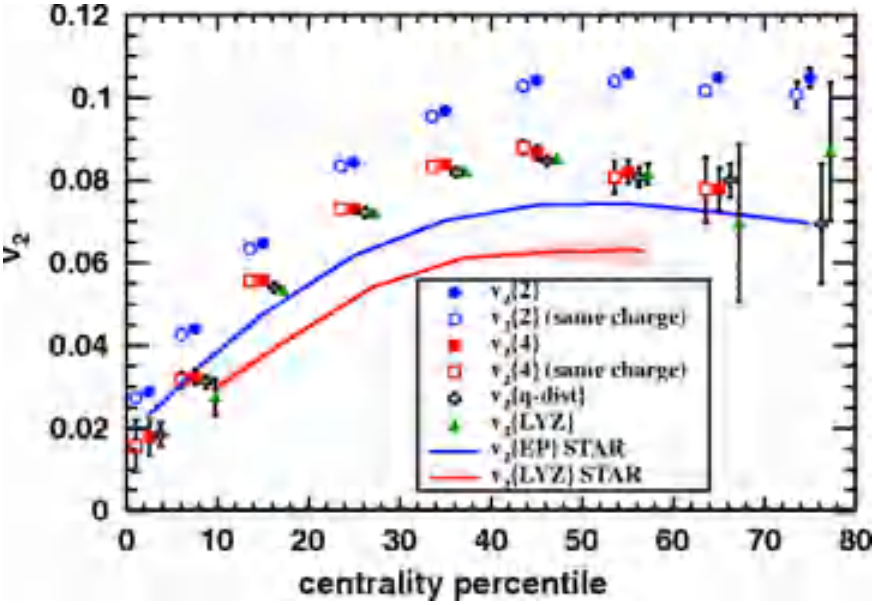

Figure 1.15: Elliptic flow integrated over the p_T range $0.2 < p_T < 5.0$ GeV/c at $\sqrt{s_{NN}} = 2.76$ TeV as a function of centrality [78]. RHIC measurements at $\sqrt{s_{NN}} = 200$ GeV is integrated over the p_T range $0.15 < p_T < 5.0$ GeV/c.

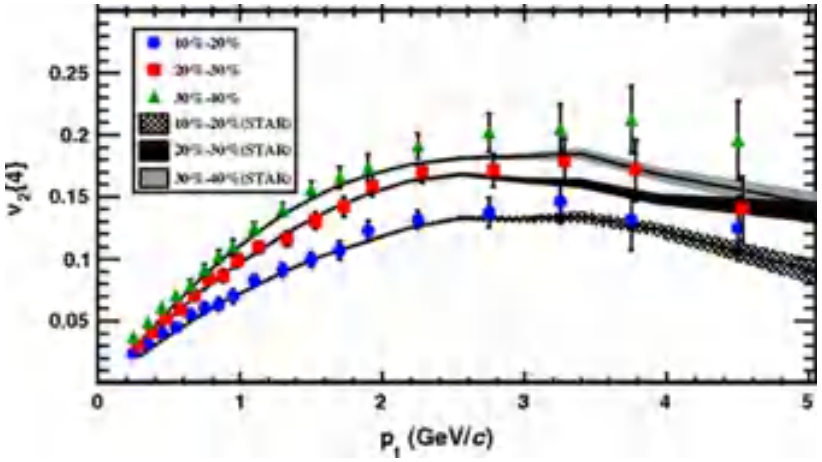

Figure 1.16: p_T dependence of $v_2\{4\}$ at $\sqrt{s_{NN}} = 2.76$ TeV for various centralities compared to STAR measurements at $\sqrt{s_{NN}} = 200$ GeV [78].

(v_2) is further examined as a function of p_T to study the evolution from RHIC to LHC. Figure 1.16 shows the p_T-dependence of elliptic flow employing the 4-particle cumulant method, $v_2\{4\}$ is measured by the ALICE group in three different centrality classes. STAR estimates are shown by dashed areas. Although a $\sim 30\%$ difference is observed between the

integrated v_2 values obtained from RHIC and LHC, the p_T differential estimates are in good agreement within uncertainties upto $p_T \approx 3.0$ GeV/c.

Thus, the increase in integrated flow at LHC can be ascribed to the increase in average transverse momentum, or in other words radial flow has a remarkable effect at high p_T and these effects can be well understood from hydrodynamic models [79, 80]. It is believed that the mutual interaction between elliptic flow and radial flow will lead to a species mass dependent p_T-differential flow. Indeed a mass ordering of v_2 at low-p_T where flow decrease with increasing hadronic mass, was observed at RHIC energy [81] as shown in the left panel of Figure 1.17. Hydrodynamic results [79] including phase transition at $T_c = 165$ MeV and kinetic freeze out at 130 MeV shown by dotted curves, are found to reproduce the mass ordering effect. Heavier particles experience a strong push towards high-p_T due to radial flow and subsequently have a smaller v_2 at a particular p_T. To put a tight constraint on radial flow and mass dependent v_2, hydro estimates from LHC and RHIC were reported together in $20 - 30\%$ centrality in [80]. Looking at the right panel of Figure 1.17 it may be inferred that v_2 of lighter particles increases but that of heavier particles decreases from RHIC to LHC energies. This results in a similar magnitude of $v_2(p_T)$ at the two collision energies which differs from each other by almost two orders of magnitude. This is one of the remarkable findings from hydrodynamic simulations. A complete review on collective flow and hydrodynamics can be found in [82, 83]. The mass ordering of v_2 at low-p_T at

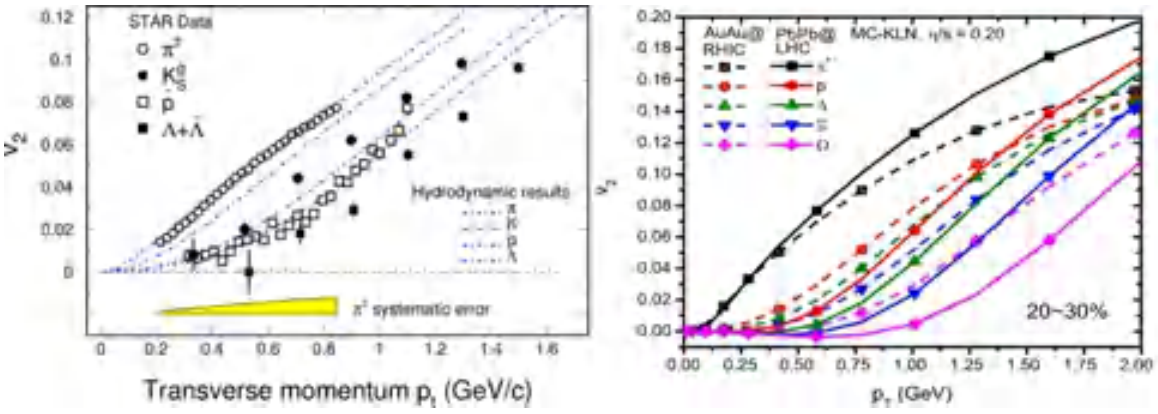

Figure 1.17: Left: Differential elliptic flow at RHIC ($\sqrt{s_{NN}} = 200$ GeV) as a function of transverse momentum compared to hydrodynamical predictions [81]. Right: Hydrodynamical prediction of differential elliptic flow for $20 - 30\%$ centrality at $\sqrt{s_{NN}} = 200$ GeV (dashed lines) and $\sqrt{s_{NN}} = 2.76$ TeV (solid lines) [80].

RHIC energies is attributed to hydrodynamic pressure gradient which further predicts that p_T-differential v_2 should scale with transverse kinetic energy defined as $KE_T = m_T - m_0$, as the driving force of elliptic flow is directly related to the collective kinetic energy of the emitted particles. Strong influence of hydrodynamic pressure gradient is confirmed from Figure 1.18 (left panel) as species-wise v_2 scales up to $KE_T \leq 1.0$ GeV/c. But the scaling

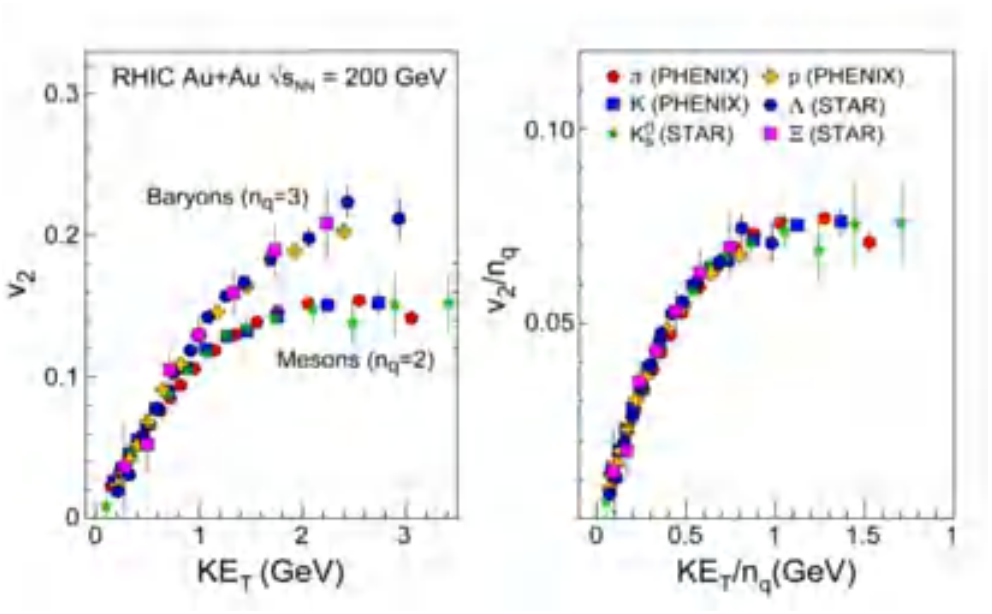

Figure 1.18: Left: v_2 against transverse kinetic energy (KE_T) for different species for minimum bias Au+Au collisions at $\sqrt{s_{NN}}$ = 200 GeV. Right: Same but after scaling by NCQ. The figure is taken from [84].

is broken for $KE_T \geq 1.0$ and clear splitting into a mesonic and baryonic branch is noted. This separate scaling is believed as a signature of presence of quarkonic degrees of freedom developed at an early stage in the flowing matter. Further to confirm the same observation, both v_2 and KE_T are divided by the number of constituent quarks (NCQ), i.e. $n_q = 3$ for baryons and $n_q = 2$ for mesons. An excellent scaling of v_2/n_q over the entire range of KE_T/n_q is depicted in the right panel of Figure 1.18. The NCQ scaling is generally explained by the quark recombination or coalescence models [85, 86]. This indicates that the system has been in a deconfined state before hadronization and is a direct evidence of partonic collectivity.

Local thermalization is one of the significant characteristics of QGP. It was predicted in Ref. [87] that the centrality and system size dependence of v_2 has the potential to examine the issues related to thermilization. Upon complete thermalization, v_2 in different systems and centrality bins would depend only on the initial anisotropy quantified as eccentricity (ε). However, in the low density limit, the mean free path is larger or comparable to the system size and the system is well away from equilibrium. Under this condition elliptic flow depends both on eccentricity and system size or centrality bins. Voloshin and Poskanzer [87] suggested that the physics of these observations can be best studied by plotting the elliptic flow parameter scaled by eccentricity (v_2/ε) as a function of transverse particle density related to the probability of interactions and quantified as $\frac{1}{S}\frac{dN_{ch}}{dy}$. It is noteworthy that eccentricity (ε) and the overlap area (S) can be computed from the Glauber model based simulations [24]. A non-smooth nature of such a plot would indicate the presence of new physics mechanism, whereas a saturation at high density would be an indication towards

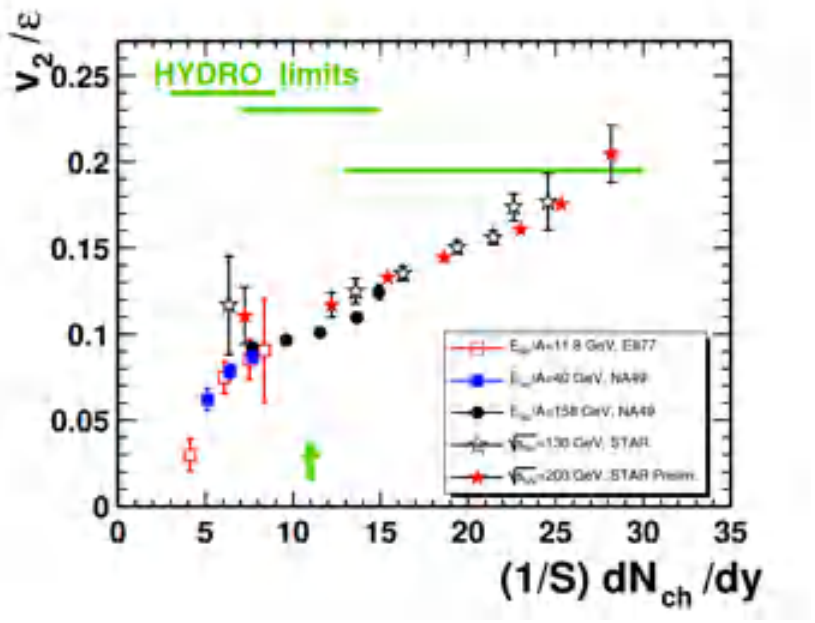

Figure 1.19: Eccentricity scaled v_2 as a function of particle density in the transverse plane at AGS, SPS to RHIC. The figure is from Ref. [88].

ideal hydrodynamic evolution. Figure 1.19 shows the eccentricity scaled v_2 plotted against $\frac{1}{S}\frac{dN_{ch}}{dy}$ over a wide range of energies from AGS, SPS, RHIC to LHC. It is observed that v_2/ε-values obtained from quite different collision systems fall approximately on a single curve. Beside that, for near central collisions at top RHIC energy, eccentricity scaled v_2 is close to the predicted hydrodynamic limit, which once again reflects that the system created in such collision having smaller mean free paths evolves towards thermalization. Another interesting

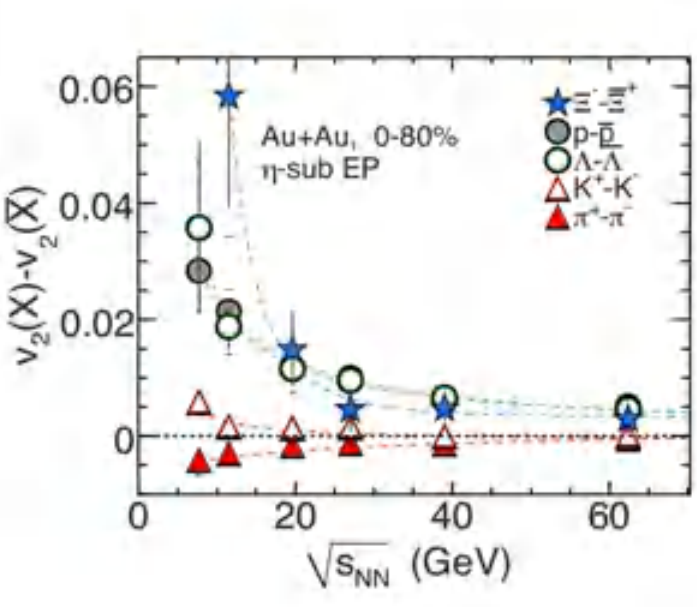

Figure 1.20: Difference in v_2 for particles and their corresponding anti-particles measured by the STAR collaboration at RHIC for $0-80\%$ central events. Dashed lines are fits to some power law function, the details of which can be found in [89].

aspect is a difference in the v_2-values for particles and antiparticles as a function of collision energy as depicted in Figure 1.20. The difference increases with increasing particle mass towards lower collision energies. The baryon chemical potential is held responsible for the observed particle dependent splitting in the elliptic flow [89]. Nevertheless, the effects of mean-field potential in both the partonic and hadronic phase are also to be considered for a meaningful explanation of the splitting [90].

In recent years the third-harmonic coefficient v_3 of the Fourier decomposition of the azimuthal distribution, also called the *triangular flow* parameter, has gained attention and has been studied extensively [91–93]. Originally it was perceived though, that due to a left-right symmetry prevailing in the transverse plane of a collision, the contribution from odd harmonics to the particle azimuthal distribution would vanish, and v_2 would be the only dominating contribution to transverse anisotropy. However, now it is widely accepted

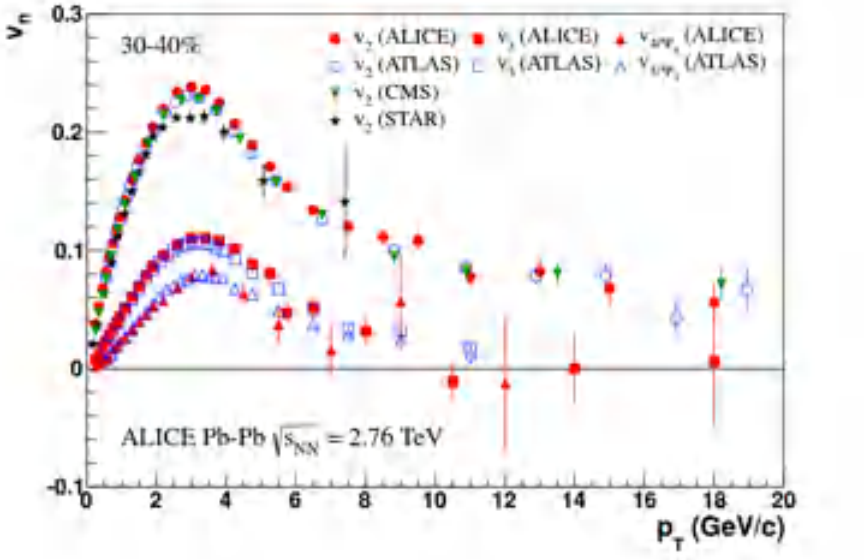

Figure 1.21: Transverse momentum dependence of different order flow harmonics (v_n) estimated by the ALICE Collaboration. [93].

that the event-by-event fluctuating position of the nucleons [94] participating in an AB collision often assumes a triangular shape, preferably called the triangularity, which with the evolution of the interacting system is converted into a momentum space anisotropy. Triangular flow is sensitive to the correlations present in the early stages of the AB collision. It has been proposed that the triangular anisotropy can explain the near side ridge and the away-side shoulder structures present in two-particle (dihadron) azimuthal correlations [91]. Furthermore, triangular flow is also believed to be sensitive to the viscous effects of the fireball medium as suggested by some simulation studies on relativistic viscous hydrodynamics [95, 96]. Transverse momentum dependence of the flow harmonics v_n for $n = 2, 3, 4$ is depicted in Figure 1.21. It is quite well understood that the signal strength of higher

harmonics decreases. A combined investigation of different orders of flow harmonics will impose significant constraints on the initial state fluctuations [96]. Further, it would be also challenging to measure the higher harmonics due to their weaker strengths, particularly in the future low-energy experiments.

1.4 CBM experiment at FAIR

In the entire landscape of heavy-ion experiments the Compressed Baryonic Matter (CBM) experiment will be of significant importance at the future Facility for Antiproton and Ion Research (FAIR), which is under construction in Darmstadt, Germany adjacent to the GSI. CBM at FAIR will facilitate the study of hot and dense matter produced in heavy-ion collisions in laboratory, but in a scenario somewhat different from its predecessors at BNL and CERN, which were devoted to investigate the properties of the strongly interacting matter at high temperature and almost zero net baryon density. The present day interest of the heavy-ion physics community is to explore the highest net baryon density region of the QCD phase diagram, which is possible only through heavy-ion collisions at moderate energies, available upto some extent at the low energy CERN-SPS experiments and will be accessible in the future FAIR facility. CBM is a dedicated fixed target experiment to collide heavy-ions in the beam kinetic energy range $2 \leq E_{\rm lab} \leq 11$ GeV/nucleon at the SIS-100 accelerator to be extended to $40A$ GeV in an upgrade to SIS-300 [97]. It has been shown

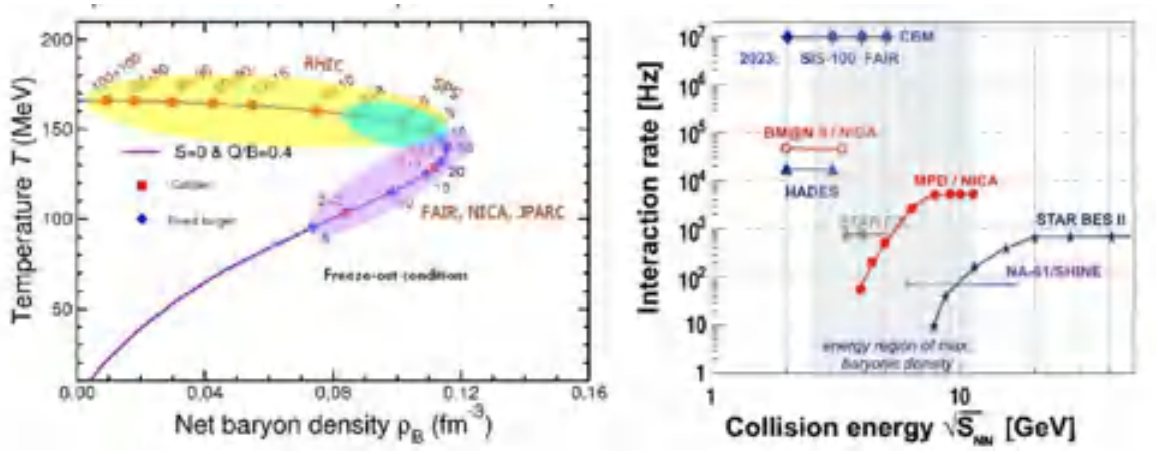

Figure 1.22: Left: Hadronic freeze out line on the temperature versus net-baryon density plane as obtained in statistical model [98]. Right: Interaction rate reached by existing and future heavy-ion experiments as a function of beam energy [99].

in [98] that the maximum net-baryon density is achievable at low SPS or FAIR energies. The observation is graphically represented in the left panel of Figure 1.22 while plotting the chemical freeze out line as a function of net-baryon density and temperature. The points represent the beam energies either in collider or fixed target experiments on Au+Au collisions. It is revealed that beam energies between 25 and $40A$ GeV are ideal to create

Table 1.2: Physics issues and their corresponding observables for the CBM experiment.

Physics Topic	**Observable**
Equation of state prevailing in high density matter	(i) Collective flow of identified particles. (ii) Production of multi-strange hadrons due to back-to-back collisions.
Restoration of chiral symmetry	Modification of the invariant mass spectra of dileptons via electron and muon channel.
Hadronic to partonic phase transition	(i) Excitation function of yield of multi-strange hyperons. (ii) Excitation function of invariant mass spectra of lepton pairs which provides an idea of the fireball temperature
Existence of critical point	Excitation function of higher order EbyE fluctuations of conserved quantities such as charge, strangeness, baryon number.
Hyperon puzzle in neutron stars [100]	Discovery of (double Λ) hypernuclei and measurement of their lifetime.

maximum net-baryon density matter. Transport calculations estimate an energy density upto 2.5 fm^{-3} and a baryon density $2-7$ times that of the normal nuclear matter at the centre of the reaction zone at this energy range. CBM comprises of an extensive examination of the observables like low mass dilepton pairs, charmonia and open charm, collective flow of both rare (multi-strange hyperons, ϕ) and bulk particles (π, p, K), correlations and fluctuations. The basic goal is to measure the rare probes inspite of their low multiplicity and small branching ratios. In order to perform measurements of the rare probes with exceptional interaction rate of upto 10 MHz the CBM detectos are designed to consist of extremely fast, ultra-radiation hard detectors and electronics [101]. For the sake of completeness apart from the CBM we list some other ongoing and future heavy-ion experiments focused to investigate the high density hadronic matter.

1. HADES at SIS18, GSI, Germany [102].
2. Nuclotron-based Ion Collider Facility (NICA) at JINR in Dubna, Russia [103].
3. STAR Fixed Target (FXT) Programme at BNL, United States [104].
4. NA61/SHINE at SPS-CERN, Switzerland [105].
5. Heavy-ion program at J-PARC in Japan (in a nascent stage) [106].

Beside CBM the reaction rates of these experimental facilities have been presented as a function of collision energy in the right panel of Figure 1.22. One should readily understand that the uniqueness of CBM experiment lies in its unparallel reaction rate in comparison to others. Moreover, the CBM detector will also be equipped with free streaming data readout and acquisition system [99]. The fundamental physics issues and their corresponding experimental observables believed to be addressed by the FAIR-CBM [99, 101] set up, is summaried in Table 1.2.

1.5 Objective of the thesis

The study of azimuthal anisotropy and collective flow of final state hadrons is believed to be one of the most important tools that can extract significant information regarding particle interactions in a hot and dense nuclear and/or partonic medium produced in high energy heavy-ion collisions. Properties of this kind of matter is supposed to be guided by the rules of QCD. Our present understanding of collective flow at FAIR energy region is constrained by the unavailability of experimental data. Though the Alternating Gradient Synchrotron (AGS) [74], Super Proton Synchrotron (SPS) [88] and some low energy RHIC measurements [107, 108] provide us with some sort of a database, it is nevertheless necessary to scan a much wider range of collision energies involving different colliding systems that may be used to study baryon rich hadronic matter where high degree of nuclear stopping is expected. In absence of substantive experimental data, simulations that are successful in describing certain phenomenon like the collective flow, can provide us with such useful information as to what can be expected in future experiments. Such an exercise will not only help us understand the dynamics of the system but will also provide us with important clues that might constrain the models/theories to be used to characterize a baryon rich fireball. Keeping this in mind, in this thesis we have studied different aspects of collective flow of charged particles produced in Au+Au collisions at the FAIR energies using the Ultra-relativistic Quantum Molecular Dynamics (UrQMD) [109], and A Multiphase Transport (AMPT) [110] model. The Monte Carlo Glauber (MCG) model [24] is employed to characterize the collision geometry at an early stage of the evolution of an AB collision. The latest available version of these models are used to simulate symmetric fixed target nuclear collisions at incident energies $E_{\rm Lab}$ = 10A, 20A, 30A, and 40A GeV. The main motivation behind this kind of simulation based analysis is to examine how different flow parameters are expected to behave in a moderate temperature, baryon-rich environment, and in what respect are they similar/different from a high temperature and almost baryon free fireball created in RHIC and/or LHC experiments. The results at high energy density and high temperature in an almost baryon free condition obtained from the RHIC and LHC experiments are available in literature. We believe that it is worthwhile to compare and supplement the RHIC and LHC results with those obtained from the present analysis of simulated data.

Bibliography

[1] S. L. Glashow, Nucl. Phys. **22**, 579 (1961).

[2] A. Salam and J. C. Ward, Phys. Lett. **13**, 168 (1964).

[3] S. Weinberg, Phys. Rev. Lett. **19**, 1264 (1967).

[4] H. Fritzsch, M. Gell-Mann, and H. Leutwyler, Phys. Lett. B **47**, 365 (1973).

[5] D. J. Gross and F. Wilczek, Phys. Rev. Lett. **30**, 1343 (1973).

[6] H. D. Politzer, Phys. Rev. Lett. **30**, 1346 (1973).

[7] K. G. Wilson, Phys. Rev. D **10**, 2445 (1974).

[8] S. Bethke, Nucl. Phys. Proc. Suppl. **121**, 74 (2003).

[9] J. Schwinger, Phys. Rev. **128**, 1, 2425 (1962).

[10] A. Casher, J. Kogut, and L. Susskind. Phys. Rev. D **10**, 1 732 (1974).

[11] A. H. Mueller, Nucl. Phys. B **213**, 85 (1983); *ibid* **241**, 141 (1983); Dokshitzer *et al.*, Z. Phys. C **27**, 65 (1985).

[12] J. C. Collins and M. J. Pery, Phys. Rev. Lett. **34**, 1353 (1975).

[13] N. Cabibbo and G. Parisi, Phys. Lett. B **59**, 67 (1975).

[14] E. V. Shuryak, Sov. Phys. JETP **47**, 212 (1978) [Zh. Eksp. Teor. Fiz.74,408(1978)].

[15] R. Hagedorn, Suppl. Nuovo Cim. **3** 147 (1965).

[16] W. Greiner, S. Schramm, and E. Stein, Quantum Chromodynamics, 2nd edition, Springer-Verlag, Germany, (2002).

[17] E. W. Kolb and M. S. Turner, The Early Universe, Addison-Wesley, USA, (1990).

[18] J. Allday, Quarks, Leptons, and the Big Bang, Taylor and Francis, UK (2002).

[19] E. V. Shuryak, Phys. Lett. B **78**, 150 (1978).

[20] G. Baym *et al.*, Rep. on Prog. in Phys. **81**, 056902 (2018).

[21] `https://www.civilsdaily.com/news/evolution-of-universe-after-the-big-bang/`

[22] T.D. Lee and G. C. Wick, Phys. Rev. D **9**, 2291 (1974).

[23] A. Toia, Cern Courier, **April**, 31 (2013).

[24] M. L. Miller *et al.*, Ann. Rev. Nucl. Part. Sci. **57**, 205 (2007).

[25] J. P. Lansberg, Physics of Ultrarelativistic Heavy-ion Collisions, Talk given in the Energy Atlas Workshop, Benasque, Spain (2015).

[26] C. Shen and U. Heinz, Nucl. Phys. News **25**, 6 (2015).

[27] https://www.Evolution of collisions and QGP/Particles and friends (wordpress.com).

[28] S. Afanasiev *et al.*, Phys. Rev. Lett. **99**, 052301 (2007).

[29] E. Fermi, Prog. Theo. Phys. **5**, 570 (1950).

[30] A. Chodos *et al.*, Phys. Rev. D **9**, 3471 (1974).

[31] A. Chodos, B. L. Jaffe, K. Johnson and C. B. Thorn, Phys. Rev. D **10**, 2599 (1974).

[32] C. -Y. Wong, Introduction to High-Energy Heavy-Ion Collisions, World Scientific, Singapore, (1994).

[33] R. Vogt, Ultrarelativistic Heavy-Ion Collisions, Elsevier, The Netherlands, (2007).

[34] A. K. Chaudhuri, A Short Course on Relativistic Heavy-Ion Collisions, IOP Publishing, UK, (2014).

[35] D. Evans, QCD and the Quark-Gluon Plasma, Talk given in the Summer School, Queen's University, Belfast, UK (2017).

[36] L. D. Landau, Izv. Akad. Nauk. Ser. Fiz. **17**, 51 (1953).

[37] S. Z. Belensky and L. D. Landau, Usp. Fiz. Nauk. **56**, 309 (1955).

[38] I. M. Khalatnikov, J. Exp. Theor. Phys. **26**, 529 (1954).

[39] P. Carruthers and M. Duong-Van, Phys. Rev. D **28**, 130 (1983).

[40] S. Pokorski and L. Van Hove, Acta. Phys. Pol. B **5**, 229 (1974).

[41] L. Van Hove and S. Pokoroski, Nucl. Phys. B **86**, 243 (1975).

[42] J. D. Bjorken, Phys. Rev. D **27**, 140 (1983).

[43] K. Yagi, T. Hatsuda and Y. Miake, Quark-Gluon Plasma, From Big Bang to Little Bang, Cambridge University Press, UK (2005).

[44] P. Kolb and U. Heinz, Quark-Gluon Plasma 3, (Eds.) R. C. Hwa and X. N. Wang, World Scientific, Singapore (2003).

[45] A. Bazavov *et al.*, Phys. Rev. D **85**, 054503 (2012).

[46] R. D. Pisarski, F. Wilczek, Phys. Rev. D **29**, 338 (1984).

[47] M. A. Stephanov, Prog. Theor. Phys. Suppl., **153** 139 (2004).

[48] F. Karsch, E. Laermann and B. Peikert, Nucl. Phys. B **605**, 579 (2001).

[49] Z. Fodor and S. D. Katz, J. High Ener. Phys. **03**, 014 (2002).

[50] Z. Fodor and S. D. Katz, J. High Ener. Phys. **04**, 050 (2004).

[51] The Frontiers of Nuclear Science, A Long Range Plan, The DOE/NSF Nuclear Science Advisory Committee, arXiv:0809.3139v1[nucl-ex].

[52] J. Pochodzalla *et al.*, Phys. Rev. Lett. **75** 1040 (1995).

[53] J. B. Elliott *et al.*, Phys. Rev. C **87**, 054622 (2013).

[54] H. Satz, The Quark-Gluon Plasma, A short introduction, Talk given in 6th International Conference on Physics and Astrophysics of Quark Gluon Plasma, Dec. 5 - 10, Goa/India, 2010.

[55] T. Matsui and H. Satz, Phys. Lett. B **178**, 416 (1986).

[56] P. Steinberg (for the ATLAS Collaboration), Quarkonia and Vector Bosons measured with the ATLAS detector at the LHC, Talk given in the BNL Quarkonia Workshop, BNL, USA (2011).

[57] M. Gonin *et al.* (NA50 Collaboration), Nucl. Phys. A **610**, 404c (1996).

[58] M. C. Abreu *et al.* (NA50 Collaboration), Nucl. Phys. A **661**, 93 (1999).

[59] A. Adare *et al.* [PHENIX Collaboration], Phys. Rev. Lett. **98**, 232301 (2007).

[60] J. D. Bjorken, Fermilan-Pub-82-059-THY, Batavia (1982).

[61] G. -Y. Qin and X. -N. Wang, Int. J. Mod. Phys. E **24**, 1530014 (2015).

[62] J. Adams *et al.* (STAR Collaboration), Phys. Rev. Lett. **91**, 072304 (2003).

[63] M. Aaboud *et al.* (ATLAS Collaboration), Phys. Lett. B **790**, 108 (2019).

[64] J. Rafelski and B. Müller, Phys. Rev. Lett. **48**, 1066 (1982).

[65] P. Koch, B. Müller, and J. Rafelski, Phys. Rept. **142**, 162 (1986).

[66] K. Aamodt *et al.* (ALICE Collaboration), Phys. Lett. B **728**, 216 (2014).

[67] F. Antonori *et al.* (NA57 Collaboration), J. Phys. G **32**, 427 (2006).

[68] B. I. Abelav *et al.* (STAR Collaboration), Phys. Rev. C **77**, 044908 (2008).

[69] A. Dumitru *et al.*, Z. Phys. A **353**, 187 (1995).

[70] J. Y. Ollitrault, Phys. Rev. D **46**, 229 (1992).

[71] H. Sorge, Phys. Lett. B **402**, 251 (1997).

[72] S. A. Voloshin and Y. Zhang, Z. Phys. C **70**, 665 (1996).

[73] A. M. Poskanzer and S. A. Voloshin, Phys. Rev. C **58**, 1671 (1998).

[74] J. Barette *et al.* (E877 Collaboration), Phys. Rev. C **55**, 1420 (1997).

[75] C. Pinkenburg *et al.* (E895 Collaboration), Phys. Rev. Lett. **83**, 1295 (1999).

[76] M. J. Tannenbaum, Universe **5(6)**, 140 (2019).

[77] K. H. Ackermann *et al.* (STAR Collaboration), Phys. Rev. Lett. **86**, 402 (2001).

[78] K. Aamodt *et al.* (ALICE Collaboration), Phys. Rev. Lett. **105**, 252302 (2010).

[79] P. Huovinen, P. Kolb, P. Ruskanen, and S. Voloshin, Phys. Lett. B **503**, 58 (2001).

[80] U. Heinz, C. Shen, and H. Song, AIP Conf. Proc. **1441**, 766 (2012).

[81] J. Adams *et al.* (STAR Collaboration), Phys. Rev. C **72**, 014904 (2005).

[82] U. Heinz and R. Snellings, Ann. Rev. Nucl. Part. Sci. **63**, 123 (2011).

[83] S. Jeon and U. Heinz. Int. J. Mod. Phys. E **24**, 1530010 (2015).

[84] A. Adare *et al.* (PHENIX Collaboration), Phys. Rev. Lett. **98**, 162301 (2007).

[85] D. Molnar and S. A. Voloshin, Phys. Rev. Lett. **91** 092301 (2003).

[86] R. J. Fries *et al.*, Phys. Rev. Lett. **90** 202303 (2003).

[87] S. A. Voloshin and A. M. Poskanzer, Phys. Lett. B **474**, 22 (2000).

[88] C. Alt *et al.* (NA49 Collaboration), Phys. Rev. C **68**, 034903 (2003).

[89] L. Adamczyk *et al.* (STAR Collaboration), Phys. Rev. Lett. **110**, 142301 (2013).

[90] J. Xu, T. Song, C. M. Ko, and F. Li, Phys. Rev. Lett. **112**, 012301 (2014).

[91] B. Alver and G. Roland, Phys. Rev. C **81**, 054905 (2010).

[92] L. Adamczyk *et al.* (STAR Collaboration), Phys. Rev. C **88**, 014904 (2013).

[93] K. Aamodt *et al.* (ALICE Collaboration), Phys. Lett. B **719**, 18 (2013).

[94] B. Alver *et al.* (STAR Collaboration), Phys. Lett. B **98**, 242302 (2007).

[95] B. Alver *et al.*, Phys. Rev. C. **82**, 034913 (2010).

[96] B. Schenke, S. Jeon, and C. Gale, Phys. Rev. C **82**, 014903 (2010); **85**, 024901 (2012).

[97] C. Simon, I. Deppner, and N. Herrmann, PoS **CPOD17**, 014 (2017).

[98] J. Randrup and J. Cleymans, Phys. Rev. C **74**, 047901 (2006).

[99] T. Ablyazimov *et al.* (CBM Collaboration), Eur. Phys. J. A **53**, 60 (2017).

[100] I. Bombaci, JPS Conf. Proc. **17**, 101002 (2017).

[101] B. Friman, C. Hohne, J. Knoll, S. Leupold, J. Randrup, R. Rapp, and P. Senger, Lect. Notes Phys. **814**, pp. 1-980 (2011).

[102] HADES Collaboration, `https://www-hades.gsi.de/`

[103] N. S. Geraksiev (for the MPD Collaboration), Phys. Conf. Ser. **1023**, 012030 (2018).

[104] K. C. Meehan (for the STAR Collaboration), J. Phys. Conf. Ser. **742**, 012022 (2016).

[105] N. Abgrall *et al.*, (NA61/SHINE Collaboration), JINST **9**, P06005 (2014).

[106] H. Sako *et al.*, Nucl. Phys. A **931**, 1158 (2014).

[107] L. Adamczyk *et al.* (STAR Collaboration), Phys. Rev. C **86**, 054908 (2012).

[108] L. Adamczyk *et al.* (STAR Collaboration), Phys. Rev. C **88**, 014902 (2013).

[109] S. A. Bass *et al.*, Prog. Part. Nucl. Phys. **41**, 255 (1998);
M. Bleicher *et al.,* J. Phys. G **25**, 1859 (1999).

[110] B. Zhang *et al.*, Phys. Rev. C **61**, 067901 (2000);
Z. -W. Lin *et al.*, Phys. Rev. C **72**, 064901 (2005).